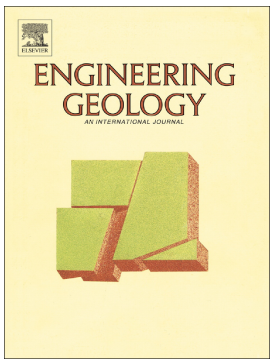

An investigation of the combined effect of rainfall and road cut on landsliding

Samprada Pradhan, David G. Toll, Nick Rosser, Matthew J. Brain

PII: S0013-7952(22)00272-1

DOI: https://doi.org/10.1016/j.enggeo.2022.106787

Reference: ENGEO 106787

To appear in: *Engineering Geology*

Please cite this article as: S. Pradhan, D.G. Toll, N. Rosser, et al., An investigation of the combined effect of rainfall and road cut on landsliding, *Engineering Geology* (2022), https://doi.org/10.1016/j.enggeo.2022.106787

An investigation of the combined effect of rainfall and road cut on landsliding

Samprada Pradhan[1,*] samprada.pradhan@durham.ac.uk**, David G. Toll**[2] d.g.toll@durham.ac.uk**, Nick Rosser**[3] n.j.rosser@durham.ac.uk**, Matthew J. Brain**[4] matthew.brain@durham.ac.uk

[1]Postdoctoral Research Associate, Department of Engineering and Institute of Hazard, Risk and Resilience, Durham University, Durham, DH1 3LE, United Kingdom.

[2]Professor, Department of Engineering and Institute of Hazard, Risk and Resilience, Durham University, Durham, DH1 3LE, United Kingdom.

[3]Professor, Department of Geography and Institute of Hazard, Risk and Resilience, Durham University, Durham, DH1 3LE, United Kingdom.

[4]Associate Professor, Department of Geography, Durham University, Durham, DH1 3LE, United Kingdom.

[*]Corresponding author.

Abstract

The reduction of soil suction and consequent loss of shear strength due to infiltration is known to trigger shallow landslides during periods of concentrated rainfall. In the mountainous terrain of Nepal, the risk of shallow rainfall-induced landsliding is further exacerbated by the non-engineered hillslope excavation for the construction of local roads. To better understand the combined effect of rainfall and road cutting on landsliding, a detailed investigation of a shallow landslide was conducted, on a site with a steep road cut that failed due to rainfall infiltration in July 2018. An integrated investigation approach was adopted, combining field and laboratory testing, and field monitoring with a series of coupled hydro-mechanical analyses with the finite element code PLAXIS 2D. The field and laboratory tests were performed to characterise the subsoil condition and determine the soil parameters for the hydro-mechanical analyses. Further, a field monitoring program was set up to obtain real-time measurements of rainfall and volumetric water content of the soil. The monitored data was used for calibration of the numerical model to assess the reliability of its predictions. Results of the numerical back-analysis suggest

that the landslide was triggered by rainfall infiltration causing a gradual reduction of soil suction at the shallow depths of ≤1.7m and the presence of the steep road cut promoted slope failure by allowing larger displacements to occur in the hillslope. Without the road cut, the slope was found to have ~35% greater initial factor of safety and under the landslide-triggering rainfall, the slope was found to remain stable with ~170% greater factor of safety than that in the slope with the road cut. This indicates that the presence of a road cut increases the likelihood of landslide during rainfall and lowers the minimum level of rainfall needed for its initiation. Hence, rainfall-induced roadside slope failures could become more frequent and extensive if roads continue to be built using informal slope excavation, without adopting suitable interventions, some examples of which are presented in this study.

Keywords: landslides, infiltration, road construction, Nepal, soil-moisture sensors, coupled hydro-mechanical analysis.

1. Introduction

Rainfall-induced landslides pose a serious threat to lives and properties around the world. The mountainous country Nepal experiences widespread landslides every year triggered by the concentrated monsoonal rainfall between June and September (Dahal and Hasegawa, 2008; Petley et al., 2007; Upreti and Dhital, 1996). The monsoonal rainfall constitutes ~80% of the total annual rainfall and studies show that more than 90% of the fatal landslides in Nepal occur during this period (Froude and Petley, 2018; NDRRMA, 2021; Petley et al., 2007). In the last decade, landslides caused the loss of over 1200 lives and economic damage of more than $14 million in Nepal (NDRRMA, 2021).

The proliferation of informal local roads in Nepal has further increased the risk of rainfall-induced landsliding (Dahal et al., 2010; Devkota et al., 2014; Froude and Petley, 2018; Mcadoo et al., 2018; Petley et al., 2007; Vuillez et al., 2018), and this has been attributed to the non-engineered or informal method of slope excavation for road construction, often crossing terrain with steep angles, without suitable planning, design and drainage and protection measures (Dixit et al., 2021; Hearn and Shakya, 2017; Robson et al., 2021; UNDP, 2011; World Bank, 2012). The study by Mcadoo et al. (2018) found that the rainfall-triggered landslides could occur with approximately twice the frequency in areas with poorly constructed

roads than in those without, based on the spatial distribution analysis of landslides and roads in Sindhupalchok district, Nepal. Vuillez et al. (2018) also found that within the Phewa watershed in western Nepal, the occurrence of landslides during extreme rainfall events was more prominent in areas intersected by or in close vicinity of the roads.

Although the association between rainfall, road construction and landslides in Nepal has been recognised anecdotally (Dahal et al., 2010; Rosser et al., 2021) and broadly correlated statistically by previous studies (Petley et al., 2007), there is limited understanding related to the physical process by which road cuts influence slope stability during rainfall. The necessity to model this physical process to better understand the combined road-rainfall effect on landsliding has also been emphasised by Mcadoo et al. (2018). Moreover, the need to address landslides related to roads and rainfall extends beyond Nepal to other low- and middle-income countries, where the construction of non-engineered steep slopes as part of road building is common and is known to be a dominant driver of instability (Haigh and Rawat, 2012; Holcombe et al., 2016; Sati et al., 2011; Sidle et al., 2014, 2011; Sidle and Ziegler, 2012).

Assessing the physical process of the rainfall-triggered landslides requires understanding how the transient atmospheric process like rainfall influences the unsaturated soil behaviour near the ground surface (Fredlund and Rahardjo, 1993). Rainfall infiltration into the unsaturated zone is known to cause an increase in the soil water content, and reductions in soil suction and shear strength (Brand, 1981; Fredlund, 1987; Godt et al., 2009; Lumb, 1975; Rahardjo et al., 2019; Springman et al., 2003; Tsaparas et al., 2002). The resulting pore water pressure changes modify the soil stresses, which causes soil deformation, and soil deformation, in turn, modifies the seepage process because the key hydraulic properties like permeability, porosity, and water retention capacity of soil change with the changes in stresses (Song and Borja, 2014; Zhang et al., 2018). Hence, the analysis of the physical process of rainfall-triggered landslides requires powerful numerical modelling methods that can model not only the effect of transient atmospheric conditions but also the interdependence between seepage and stress-deformation for unsaturated soils.

The coupled hydro-mechanical analysis effectively captures this interdependence by allowing simultaneous computation of both hydraulic and mechanical responses of variably saturated soils, which is necessary for the accurate assessment of rainfall-induced landslides (Chen et al., 2018; Hamdhan and

Schweiger, 2013; Laloui et al., 2016; Md. Rahim and Toll, 2014; Qi and Vanapalli, 2015; Yang et al., 2017, 2019; Yubonchit et al., 2017). Compared to the uncoupled analyses, where the hydraulic and mechanical aspects of soil behaviour are treated separately, the coupled hydro-mechanical analyses have been reported to provide a better prediction of factor of safety and the pore water pressure predictions from coupled analyses have been found to be in good agreement with field-measured pore water pressures (Hamdhan and Schweiger, 2013; Toll et al., 2019). Studies have also shown that the coupled analyses can closely predict actual failure times, in addition to providing a better prediction of seepage and stress distribution (Md. Rahim, 2016; Oh and Lu, 2015; Yang et al., 2017, 2020, 2019).

Thus, addressing the need to understand the physical process of landslides triggered by the combined effect of rainfall and road cut in Nepal, and considering the advantages of the coupled hydro-mechanical analyses, this study utilises the hydro-mechanical approach to investigate a case study of a rainfall-induced landslide on a road cut slope in Sindhupalchok district, Nepal. Using this case study, this paper aims to 1) back-analyse the landslide to understand the underlying mechanism and physical processes involved in the failure and 2) quantitatively assess the effect of the road cut on the occurrence of the landslide during rainfall. Through a series of numerical analyses, this study also attempts to demonstrate the viability of coupled hydro-mechanical analyses to capture the hydrological changes in unsaturated soils due to soil-atmospheric interaction and to predict the occurrence of slope failures. As hydro-mechanical modelling requires a good understanding of the relevant physical, mechanical, and hydraulic soil parameters, comprehensive field and laboratory testing of the soils were conducted during this study. The field and laboratory data were used to define the input material properties for numerical modelling. A field hydrological monitoring program was also undertaken at the study site after the landslide, and the monitored data was utilised to calibrate the numerical model to ensure reliable prediction of the slope response to rainfall and drying can be made for the periods without available monitoring data.

2. Study area

The investigated landslide is located in Kanglang village in the Upper Bhote Koshi valley of Sindhupalchok district, Province 3, Nepal (hereafter referred to as the Kanglang landslide) (Fig. 1a). During the widening of the local road from Daklang to Listi (Fig. 1b), the slope was informally excavated

to a steep ~70° cut in December 2017 (Fig. 1c). It is common for slopes to be excavated at steep angles during the construction of local roads to minimise earthwork volumes and associated costs (Hearn, 2011). During the following monsoon in July 2018, a translational slide (Varnes, 1958) occurred, affecting a larger area above the road cut (Fig. 1d). With ~1.5 m depth of the sliding surface, the landslide can be categorised as a shallow translational slide. The length and width of the landslide are approximately 25 m (upslope), and 45 m (along slope) respectively. The sliding soil body generally followed the Northeast direction, extending from an elevation of 1440 m (toe) m to 1460 m (crown) above sea level (a.s.l.). The elevations were recorded using a hand-held GPS (Garmin 60CSx), which provides an approximate estimation of the elevation with an accuracy of <10 m. Although the exact timing of the landslide is not known, the landowner noted that the landslide occurred before 16 July 2018.

The study area receives an average of 3599 mm of rainfall annually, the second-highest rainfall in Nepal (Karki et al., 2016), based on the 64-year rainfall record (1955-2018) at the nearest weather station in Gumthang, located ~6.3 km from the study site (DHM, 2018). The topography of the region is rugged with steep slopes, narrow gorges and high relief with altitudes ranging from 760 to 4100 m (Tanoli et al., 2017). Geologically, the Kanglang landslide is underlain by a thick colluvial deposit with a mix of gravel-, cobble-, and boulder-sized materials, near the middle section of a hillslope which could be an ancient landslide deposit (Fig. 1b). Such deposits encountered on the mountain slopes are formed by progressive downslope transport of materials from gravity-driven mass movement or hill wash processes (Hearn, 2011). The study site is approximately 7.4 km south of the Main Central Thrust (MCT) and the region south of MCT is dominated by sedimentary and metasedimentary rocks including shale, sandstone, limestone, dolomite, slate, phyllite, schist, and quartzite (Upreti, 2001). The majority of the Daklang-Listi road, including the Kanglang landslide, traverses through the Lakharpata formation (DMG, 1994), which includes Malekhu limestone, Benighat slate, and Dhading Dolomites of the Upper Nuwakot unit (Stöcklin, 1980; Upreti, 1996). During the 2015 Gorkha earthquake, Nepal, Sindhupalchok district was severely affected by a large number of co-seismic landslides (Kincey et al., 2021; Roback et al., 2018). The consequent post-earthquake landslide activities in this region have been reported to have remained active and evolving by recent studies (Kincey et al., 2021; Tian et al., 2020). Due to the combination of heavy rainfall, rugged topography, proximity to the tectonic fault, post-earthquake landslide activity, as well as

ongoing anthropogenic activities like road-building (Mcadoo et al., 2018; Rosser et al., 2021), the study area is susceptible to both natural and anthropogenic landslides.

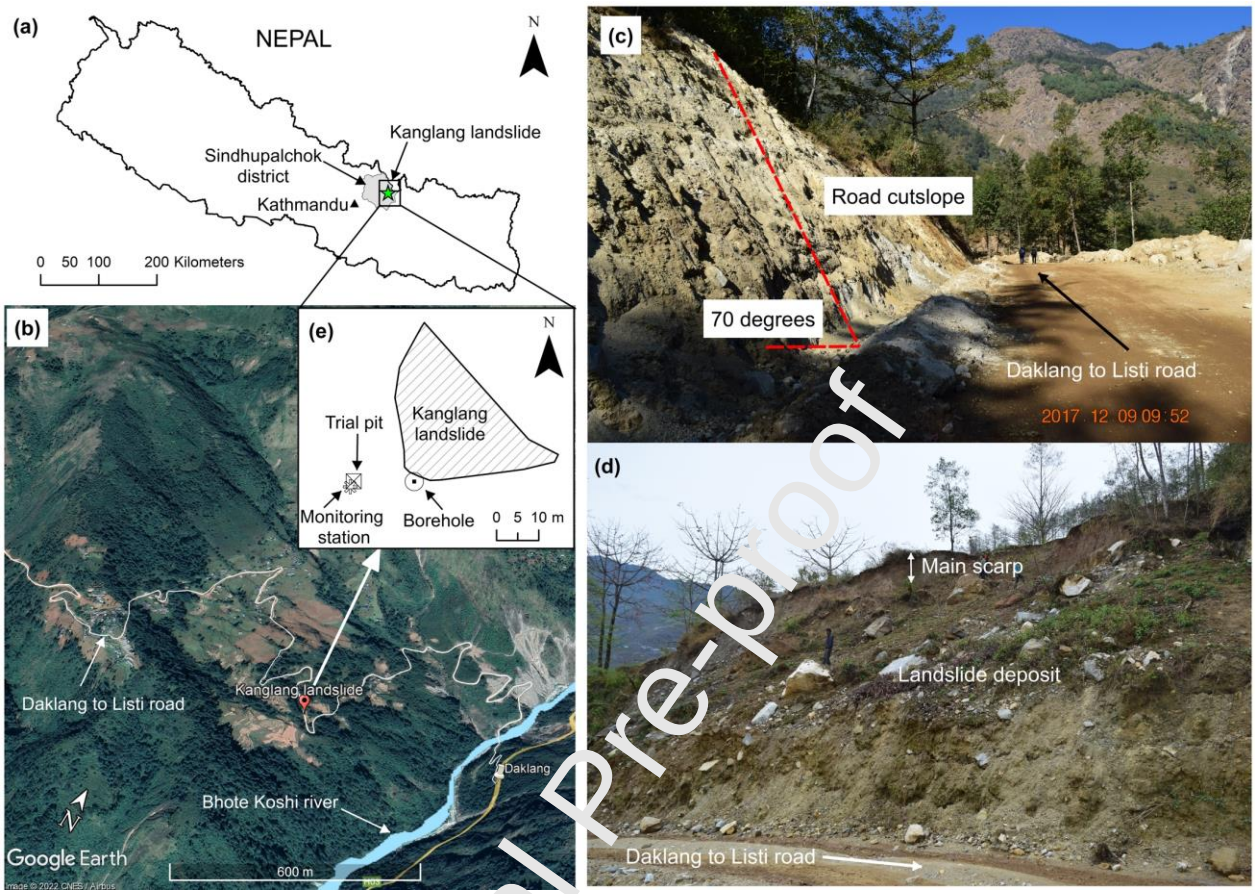

Fig. 1 (a) Map of Nepal showing the location of the Kanglang landslide within Sindhupalchok district, (b) location of the landslide along Daklang-Listi road, (c) road cut slope before the landslide, (d) road cut slope after the landslide, and (e) Kanglang landslide perimeter showing the locations of the borehole, trial pit and monitoring station.

3. Methodology

There are three key steps in the adopted methodology. First is the detailed geotechnical field investigation, where borehole drilling, standard penetration tests (SPTs), and trial pit excavation were conducted near the landslide crown to investigate and reconstruct the subsoil condition of the slope before the landslide. Soil samples were obtained from the borehole and trial pit for geotechnical characterisation and estimation of their mechanical (shear strength parameters) and hydraulic soil properties (SWRCs and saturated permeability). A detailed description of the methods and results of the field and laboratory testing are presented in section 5. Second is the field monitoring program conducted to assess the in-situ

hydrologic changes in the soil using real-time measurements of rainfall and volumetric water content of the soil (section 6). Finally, in the third step, using the estimated soil parameters, the failed slope was reconstructed and a series of hydro-mechanical analyses (or fully coupled flow-deformation analysis) was performed in the finite element code PLAXIS 2D (Bentley Systems Inc., 2018), the details of which is illustrated in Fig. 2.

The first part of the numerical analysis- model calibration, constituted a hydro-mechanical (or flow-deformation) analysis, where the monitored rainfall in July 2019 was imposed as a hydraulic boundary at the ground surface (Fig. 2). The predicted volumetric water content responses were compared to the in-situ volumetric water content measurements to calibrate the numerical model. Since the hydrological conditions of the slope are not known when the landslide occurred, model calibration is the crucial first step necessary to make reliable predictions of the slope behaviour under different rainfall scenarios. As shown in Fig. 2, the calibrated model was adopted for the subsequent analyses to 1) evaluate the stability of the slope from the time when the road cut was excavated in December 2017 to June 2018, before the Kanglang landslide to check if the slope is predicted to remain stable before the main landsliding event in July 2018 (stability analysis before the Kanglang landslide), 2) back-analyse and predict the failure timing and mechanism of the Kanglang landslide (back-analysis of Kanglang landslide), and 3) investigate the influence of the road cut on the landslide by replicating the back-analysis on a model representing an idealised slope without the road cut, which was subjected to the same rainfall conditions that triggered the Kanglang landslide (slope stability analysis without road cut). These numerical analyses from (1) to (3) were conducted by combining the hydro-mechanical analysis with the safety analysis to estimate the factor of safety (FOS) at different time steps (Fig. 2).

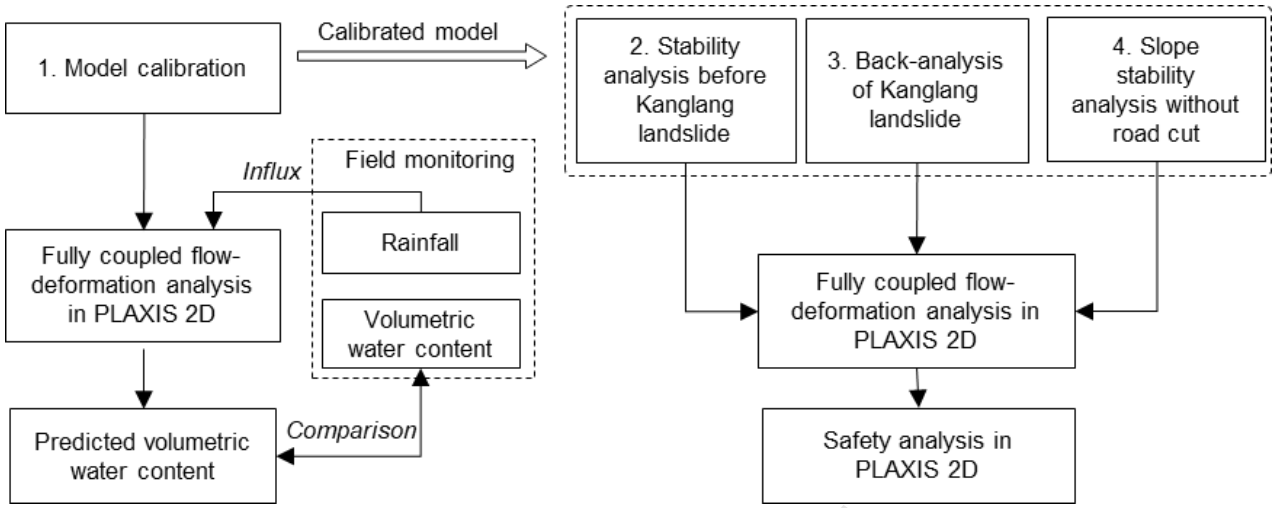

Fig. 2 Numerical modelling approach

4. Theoretical background

4.1 Coupled hydro-mechanical analysis

PLAXIS 2D was adopted in this study given its proven ability to assess the hydro-mechanical behaviour of slopes under transient hydraulic boundary conditions (Hamdhan and Schweiger, 2013). The formulation of the coupled hydro-mechanical analysis in PLAXIS is based on Biot's 3-dimensional consolidation theory (Biot, 1941), which combines the equilibrium equation and the continuity equation of the soil-water matrix (Galavi, 2010; Galavi et al., 2009). This allows computation of both deformation and groundwater seepage simultaneously under steady and transient flow boundaries in both saturated and unsaturated soil conditions (Galavi, 2010; Galavi et al., 2009). In the coupled formulation in PLAXIS, the mechanical behaviour of unsaturated soil is modelled using Bishop's effective stress concept, where the net stress and suction components are combined into single effective stress, as shown in Eq. (1) (Bishop, 1959). Under this concept, the suction coefficient χ is related to the degree of saturation and can be considered as a scaling parameter determining the contribution of matric suction to the shear strength of the unsaturated soil. In PLAXIS, χ is considered equivalent to the effective degree of saturation, and the pore water pressure is assumed to be negligible (Eq. (2)).

$$\sigma' = (\sigma - u_a) + \chi(u_a - u_w) \quad 1)$$

$$\sigma' = \sigma - S_e u_w \quad (2)$$

$$S_e = \frac{S - S_r}{S_s - S_r} \quad (3)$$

Where σ and σ' are the total and effective stresses respectively, u_a and u_w are the pore air and pore water pressures respectively, $(\sigma - u_a)$ is the net normal stress, χ is the suction coefficient, $(u_a - u_w)$ is the matric suction and S, S_e, S_r, and S_s denote the degree of saturation, effective degree of saturation, degree of saturation at residual state and degree of saturation at fully saturated state, respectively.

It is recognised that studies have questioned the suitability of Bishop's effective stress concept, particularly the consideration of the suction coefficient (χ) being a function of the degree of saturation (Fredlund et al., 1978; Jennings and Burland, 1962; Khalili and Khabbaz, 1998). However, the use of Bishop's effective stress for modelling unsaturated soil behaviour allows an easier transition between unsaturated and saturated states and studies have provided evidence of its validity, which includes one of the earliest experimental studies by Bishop and Blight (1963) on clayey soils. Toll (2020) also showed that Bishop's effective stress concept is valid for clayey soils when the degree of saturation is ≥75%. For non-clayey soils, Öberg and Sällfors (1997) found that the χ-parameter can be replaced by the degree of saturation when it is greater than ~50%. In agreement with this study, Alonso et al. (2010) and Casini et al. (2011) also found that the unsaturated soil behaviour, particularly for granular soils like sands and silts, can be expressed using a single Bishop's effective stress. Hence, whilst the Bishop's effective stress concept may not be valid for all soil types, at all ranges of saturation (Toll et al., 2019), it is reasonable to assume that for non-clayey soils, this concept can provide a realistic prediction of the unsaturated soil behaviour, particularly when the degree of saturation is high and the air phase is discontinuous, as would be the case in the modelling of rainfall-induced landslides.

As for the hydraulic behaviour of unsaturated soil in PLAXIS, the van Genuchten model (van Genuchten, 1980) was used. Based on this model, the relationship between matric suction and volumetric water content of the soil is expressed as Eq. (4) and the permeability function can be expressed as Eq. (5).

$$\theta_e = \frac{\theta - \theta_r}{\theta_s - \theta_r} = \frac{1}{\left[1 + (\alpha\psi)^n\right]^m} \quad 4)$$

Where θ is the volumetric water content, θ_e is the normalised volumetric water content, θ_r and θ_s are the volumetric water contents at residual and fully saturated states respectively, ψ is the matric suction head, and α, n, m and l are the curve fitting parameters where $m = 1 - 1/n$.

$$k = k_s k_r = k_s \theta_e^{\,l}\left[1 - (1 - \theta_e^{\,1/m})^m\right]^2 \quad 5)$$

Where k, k_s and k_r denote the coefficient of permeability, saturated coefficient of permeability and relative permeability, respectively, θ_e is the normalised volumetric water content, and α, n, m and l are the curve fitting parameters where $m = 1 - 1/n$.

4.2 Safety analysis

The safety analysis in PLAXIS uses the strength-reduction method to determine the factor of safety (Brinkgreve et al., 2018). Assuming a Mohr-Coulomb failure criterion, this method entails an incremental reduction of the shear strength parameters (cohesion and angle of shearing resistance) by a strength reduction factor until the slope reaches a failure state (Cai and Ugai, 2004; Griffiths and Lane, 1999; Matsui and San, 1992). The factor of safety is defined as the ratio of the shear strength parameters of soil to those at failure as shown in Eq. (6)

$$FOS = \frac{c'}{c'_{failure}} = \frac{tan\phi'}{tan\phi'_{failure}} \quad 6)$$

Where *c'* and ϕ' are the effective cohesion and effective angle of shearing resistance. The subscript '*failure*' denotes the shear strength parameters at failure.

5. Detailed investigation of subsoil condition and soil properties

5.1 Subsoil condition

To assess the subsoil condition, a borehole was drilled using rotary drilling next to the landslide crown (Fig. 1e). During drilling, boulder- and cobble-size materials were encountered at 5.8 and 6.3 m depths, typical for colluvial soils. SPTs were conducted in the borehole in accordance with BS EN

ISO22476-3 (BSI, 2005) at 1 m intervals to a maximum depth of 7 m. At 7 m, the SPT sampler was replaced by a solid 60° cone (SPT (cone)) to prevent damage to the sampler by the coarser materials, as recommended in BS 5930: 2015 (BSI, 2015). The number of blows required for 300 mm penetration with the cone was converted to the corresponding SPT N-value using the correlation proposed by Mohan et al. (1970). The SPTs revealed a uniform deposit of medium dense soil from 0 to 7 m with corrected SPT values ($(N_1)_{60}$) ranging from 11 to 19 (with a mean of 14) (Fig. 3). The soil samples extracted from the upper 2, 4 and 5 m exhibited reddish-brown colour and sandy to silty texture, and below 6 m, the soil was brownish grey with a sandy texture. Based on the correlation with SPT proposed by Hatanaka and Uchida (1996), the angle of shearing resistance of the soil was estimated to range from 35° to 40° (37° on average) and the elastic modulus of soil was estimated to be between 6 to 8 MPa, based on the empirical correlation given by Bowles (1997).

To obtain disturbed and undisturbed samples, a trial pit (1.5 m × 1.0 m) was excavated to 1.5 m depth as per BS ISO 18400-102:2017 (BSI, 2017) (Fig. 1e). The materials excavated from the trial pit were predominantly fine-grained and indicated the presence of silty and sandy soils. Within the trial pit, the upper 0.25 m layer exhibited a slightly different grayish-brown colour, as shown in Fig. 4 which could be due to weathering and the presence of organic matter. Below this layer, the soil was described as slightly wet, reddish-brown sandy to silty soil. From the trial pit, disturbed bag samples were collected, and core samples were obtained using open ended steel sampling tubes (ϕ 37 mm), which were driven into the bottom of the trial pit at 0.5, 1, and 1.5 m depths. After extracting the cores, the open ends were sealed with paraffin wax and wrapped in cling film to minimise moisture loss during transport. With permission from the Department of Mines and Geology, Kathmandu, Nepal, all the samples were exported to Durham University, UK for testing.

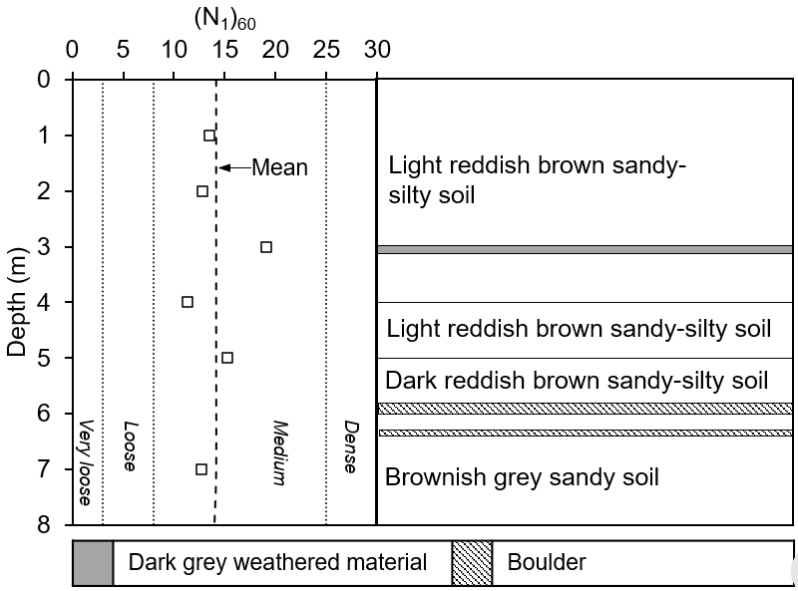

Fig. 3 Borehole SPT $(N_1)_{60}$ profile and material type.

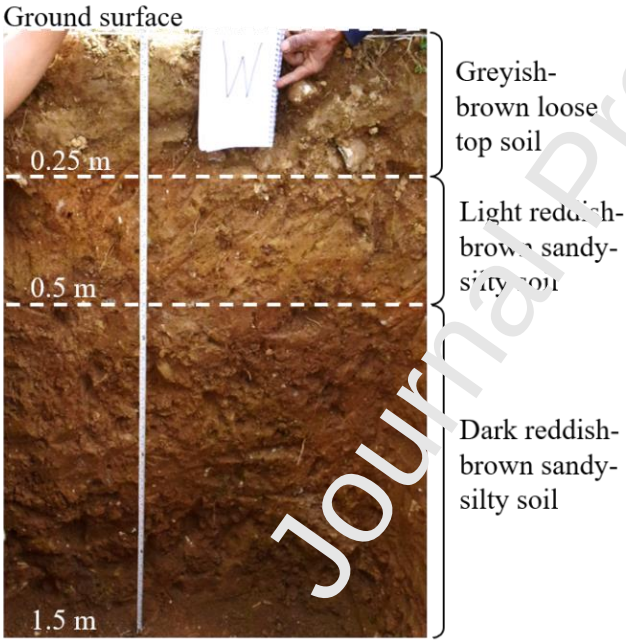

Fig. 4 Soil stratification observed in the trial pit.

5.2 Soil properties

Table 1 presents a summary of the in-situ physical properties of the core samples obtained from the trial pit. The particle size distributions were obtained using the commercial laser diffraction particle size analyser (LS 13 320) with a measurement range from 0.04 μm to 2 mm. The soil samples contained ≤12% clay-sized particles, while silt- and sand-sized particles dominated the distribution (SILT to Sandy SILT as

per BS 5930:2015 (BSI, 2015)). The samples obtained from the borehole also contained low clay contents ≤8% and higher percentages of silt-sized particles (43 to 70%). The Atterberg limits were determined as per BS EN ISO 17892-12:2018 (BSI, 2018a), where the finer fraction (<0.425 mm) of the soil samples from shallow depths (<1 m) exhibited intermediate plasticity with the plasticity index from 14 to 17% and liquid limit from 37 to 40%. The lower plasticity index and smaller clay fraction suggest a lower potential for swelling and shrinkage due to changes in water contents. Further, the sample near the ground surface was found to be relatively loose with a higher void ratio that decreased with increasing depth. The degree of saturation increased with depth, confirming the observation of a wetter soil layer below 0.5 m within the trial pit (Fig. 4).

Table 1 In-situ soil properties obtained from the core samples

Depth (m)	Clay, Silt, Sand (%< Volume)	Soil description	Particle density (Mg/m^3)	Bulk density, ρ_{bulk} (Mg/m^3)	In-situ water content, w (%)	Dry density, ρ_{dry} (Mg/m^3)	Void ratio, e	Degree of saturation, S (%)
0.5	12, 63, 25	SILT	2.72	1.57	18	1.33	1.04	47.1
1.0	8, 60, 32	SILT	2.78	1.85	17.7	1.57	0.77	64
1.5	8, 54, 38	Sandy SILT	2.75	1.98	13.3	1.75	0.57	64.2

A series of consolidated undrained (CU) triaxial compression tests were performed according to BS EN ISO 17892-9:2018 (BSI, 2018b) to estimate the shear strength parameters of the soil. The tests were performed on reconstituted soil samples obtained from 0.5 to 0.75 m depth. The samples were compacted in the laboratory to a dry density of 1.34 Mg/m^3 corresponding to the in-situ dry density of the undisturbed soil sample obtained from 0.5 m depth (Table 1). Based on the results shown in terms of the stress path plotted in the two-dimensional *p'* (mean effective stress) and *q* (deviator stress) space (Fig. 5), the critical angle of shearing resistance was estimated to be 36° (slope of the critical state line M=1.47), which is much lower than the road cut slope angle at the investigated site (~70°). The estimated angle of shearing resistance is comparable to the empirical estimation of 35° to 40° corresponding to the SPT $(N_1)_{60}$ values, as per Hatanaka and Uchida (1996). There is some evidence of a cohesive component of strength from the

tests carried out at confining stresses of 25 and 50 kPa, and the strength envelope shown in Fig. 5 represents a lower bound strength envelope.

The saturated coefficient of permeability was determined using the standard triaxial constant head permeability test as per BS EN ISO 17892-11:2019 (BSI, 2019). The test was performed by consolidating the saturated sample at 100, 200 and 300 kPa and measuring the flow through the sample at each consolidation pressure. A constant water pressure difference of 20 kPa was maintained to allow flow from the top to the bottom of the sample. With the increasing levels of the effective consolidation pressure, the saturated permeability of the soil samples was found to decrease from 1.17×10^{-7} and 1.43×10^{-8} m/s, typical for silts and silty sands (Lu and Likos, 2004).

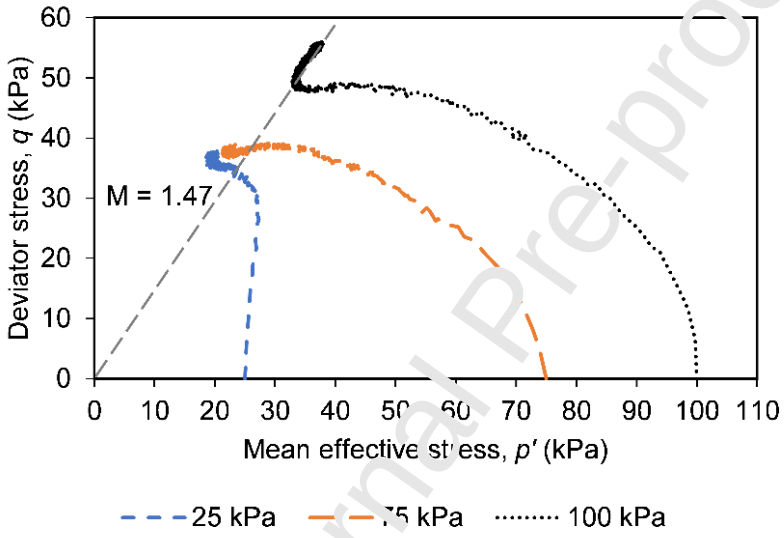

Fig. 5 *p'*-*q* stress paths obtained from the saturated CU triaxial tests

The soil-water retention curves (SWRCs) were obtained using discrete or staged drying and wetting methods as described by Lourenço et al. (2007). The soil suction was measured using the high capacity tensiometer developed at Durham University, known for its fast response rate and high suction measurements up to 2 MPa (Lourenço et al., 2006; Toll et al., 2013). Direct measurement of suction using tensiometers avoids the calibration errors that may be inevitable in other indirect suction measurement methods (Lourenço et al., 2006; Toll et al., 2013). During the test, the samples were dried and wetted in stages and were left to equalise for at least 24 hours in an insulated setting before measuring suction. After equalisation, suction was measured, and volumetric measurements of the samples were made using a digital calliper with ±0.01 mm accuracy. This process was repeated to define both the drying and wetting

SWRCs. The wetting SWRC was obtained by air-drying the sample to <1.5% water content before wetting back up to define the primary wetting curve. A wetting-scanning curve was also obtained by wetting from the end of the drying phase which was stopped at a volumetric water content of ~20%. Fig. 6a and b illustrate the SWRCs of the tested samples fitted to the van Genuchten model (VG model) (van Genuchten, 1980) (Eq. (4)). The resulting curves exhibited hysteretic behaviour during drying and wetting where the wetting-scanning curve obtained from wetting the sample after the end of the drying stage reaches the primary wetting curve. The curve fitting parameters for the van Genuchten model are also shown in Fig. 6a and b.

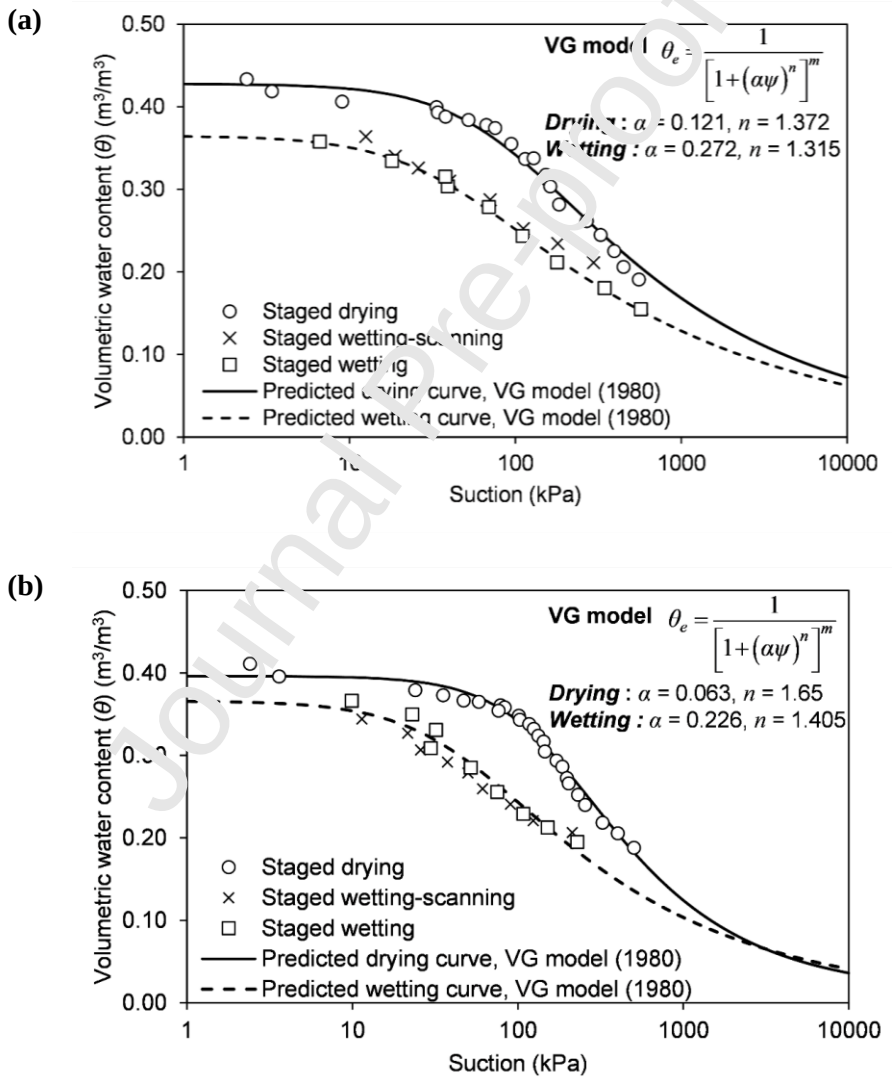

Fig. 6 Soil-water retention curves of the samples from (a) 0.3 to 0.5 m (b) 0.75 to 1 m depths.

6. Field monitoring program

During this study, a field monitoring station was established ~10 m west of the landslide crown as shown in Fig. 1e. Three 10HS soil moisture sensors (S-SMx-M005) (ONSET, 2018) were installed horizontally at depths of 0.3, 0.8, and 1.2 m on the undisturbed vertical wall of the trial pit to measure the changes in volumetric water content of the soil. The first sensor was installed at 0.3 m to capture the immediate volumetric water content soil responses while avoiding the upper layers where the plant roots could create preferential flow paths. Below this depth, the sensors were installed at vertical spacings of 0.4 to 0.5 m. The monitoring station was equipped with a rain gauge (HOBO® S-RGB-M002) (ONSET, 2018) and a data logger and telemetry system (HOBO RX3000) (ONSET, 2019) was installed to record and remotely retrieve the rainfall and volumetric water content measurements. A detailed description of the monitoring station setup is presented by Pradhan et al. (2020).

7. Numerical model set-up

7.1 Geometry

Fig. 7a shows the simplified 2-dimensional plane strain model of the investigated slope before the Kanglang landslide. The finite element mesh consisted of 3399 15-noded triangular elements and 27,515 nodes. A finer mesh was defined closer to the ground surface as higher deformation is expected in this part of the model. Additionally, the finer mesh near the ground surface was crucial to obtaining a refined prediction of the volumetric water content changes during model calibration, given that the vertical spacing between the 10HS sensors in the field was relatively small (0.4 to 0.5 m). At greater depths, the mesh size was increased to reduce computational time. Similarly, for the slope stability analysis without the road cut, a 2-dimensional plane strain model representing an idealised undisturbed hillslope was created with a finite element mesh consisting of 3623 triangular elements and 29,303 nodes (Fig. 7b). The specification of the mesh was kept identical to that in Fig. 7a so that the resulting factor of safety was comparable to that for the actual slope with the road cut.

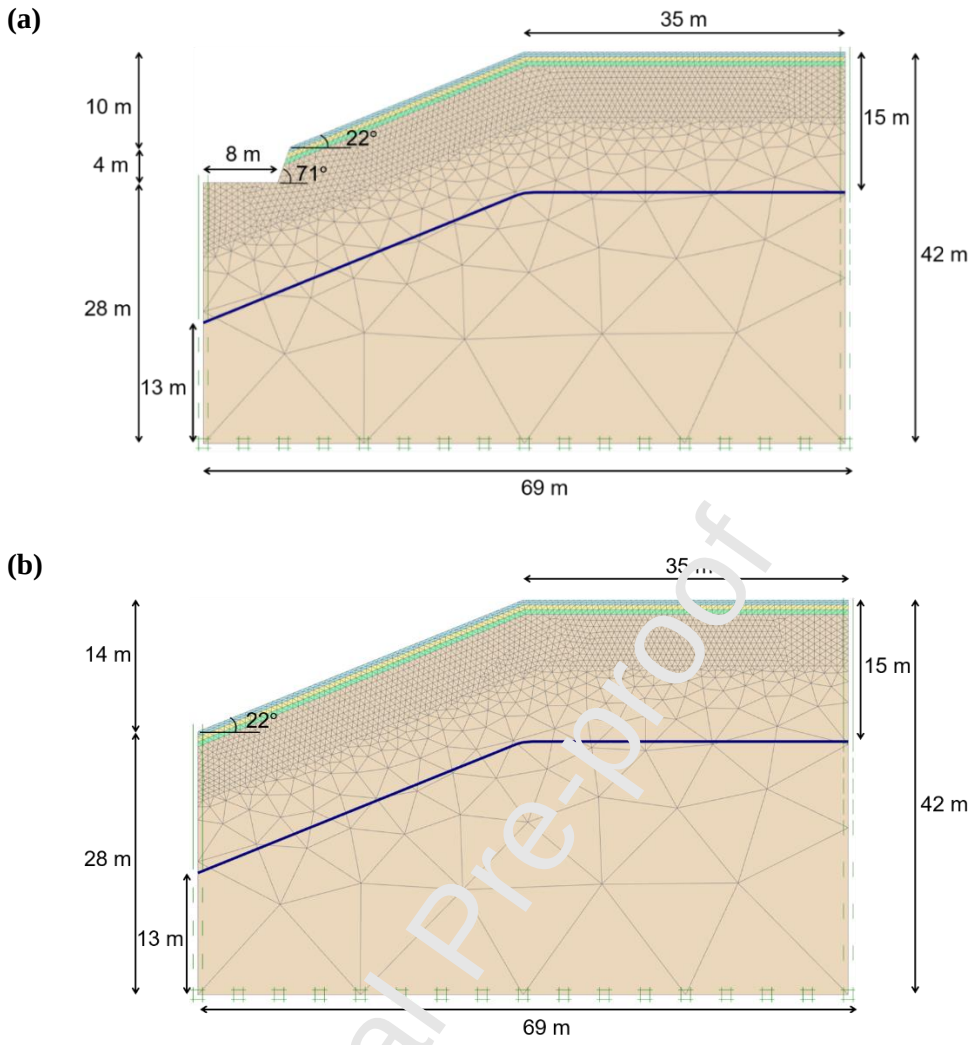

Fig. 7 Geometry of the finite element mesh for (a) the investigated slope and (b) the investigated slope without the road cut.

7.2 Material parameters

Table 2 presents the summary of the input soil parameters adopted in the numerical analyses. The four soil layers defined in Table 2, also shown in Fig. 7a and b were differentiated based on their hydraulic soil properties. The rationale for this layering was to capture the different hydrologic responses of the soils observed at the three measured depths of 0.3, 0.8, and 1.2 m during field monitoring, which are related mainly to the differences in their hydraulic properties (Fig. 8a, b and c). As the permeability tests in the laboratory were conducted at higher effective confining pressures (section 5.2), the saturated permeabilities of soil layers at shallow depths were estimated by extrapolating the measured relationship between saturated permeability and effective confining pressures. Further, the weathering and plant roots

create non-capillary macropores and surficial cracks near the ground surface, which results in a higher in-situ permeability than that measured in the laboratory (Collison et al., 1995; Dixon et al., 2019). To incorporate this within the numerical models, Toll et al. (2019) and Gasmo et al. (2000) introduced a surficial soil layer with a higher vertical permeability than the laboratory-measured value. Rouainia et al. (2009) also found a good agreement between model predictions and field-measured pore water pressures when the measured soil permeability was increased by one to two orders of magnitude. In this study, to consider the macroscopic effects near the ground, two times higher permeability than the estimated value was assigned to the top layer from 0 to 0.5 m, which provided a good agreement between predicted and measured volumetric water content responses, which is discussed further in section 8.1.

With regards to the SWRCs, it is debated in the literature whether the wetting or drying SWRC should be implemented for rainfall-induced slope stability analyses when hydraulic hysteresis cannot be taken into account. Considering infiltration corresponds closely to soil wetting, it is rational to adopt the wetting SWRC, which has also been suggested by Krisdani et al. (2019) and Kim et al. (2018). Li et al. (2005) also found a closer match between field-measured SWRC and the wetting SWRC obtained from testing. Hence, as hydraulic hysteresis cannot be modelled in PLAXIS, in all the numerical analyses presented in this study, the wetting SWRC parameters were adopted to model the hydraulic soil behaviour for both the drying and wetting phases. An exception to this is the stability analysis before the Kanglang landslide (Fig. 2), which included a prolonged dry period from 1 December 2017 to 28 February 2018, with only a few days of non-zero rainfall (Fig. 9a). For this period, the drying SWRC was used to model the hydraulic behaviour and after the end of this dry period, from 1 March 2018 to 30 June 2018, the wetting SWRC parameters were assigned to the soil layers to model infiltration. The drying and wetting SWRCs for layers 1 and 2 shown in Table 2 were measured in the laboratory (Fig. 6a and b). The value of g_a for the lower layers (layers 3 and 4) was adjusted to match the initial volumetric water content in the model to that measured in the field at 1.2 m. As the air-entry value tends to increase with the increase in normal stress and decrease in the void ratio (Miller et al., 2008), a lower value of g_a than the upper layers can be considered to be a reasonable assumption.

The conventional Mohr-Coulomb model was used to represent the constitutive relationship of all soil layers defined in Table 2. Since a uniform subsoil profile was revealed by the SPT results (Fig. 3) and a

similarly uniform subsoil was exposed inside the trial pit with only a noticeable change in colour due to weathering and wetness (Fig. 4), the shear strength properties estimated from the laboratory (Fig. 5) were considered to be uniform. Since the samples did not exhibit a distinctive peak but showed a contractive behaviour indicated by the increase in pore water pressures under undrained conditions, which is typical for loose or normally consolidated soils (OCR ~1) (Fig. 5), the angle of shearing resistance at the critical state was adopted for modelling. As the silt-sized particles dominate the particle size distribution of the soils at shallow depths (Table 1), a residual state created due to clay particles aligning within the shear zone would not be expected (Skempton, 1985). Although at the critical state, the effective cohesion is negligible, a small value of cohesion (3 kPa) was assigned to prevent numerical instabilities mainly near the ground surface where the effective stresses are lower. A smaller value of cohesion predicted localised failure near the steep face of the cut slope, which essentially was modelling surface ravelling, and this prevented the analysis of a deeper failure from proceeding further. A small cohesion of 3 kPa could be justified by the evidence of a cohesive element of strength indicated by the triaxial tests at lower stress levels, which would be relevant for shallow slope failures.

Table 2 Summary of soil properties adopted in numerical modelling

Soil layers		1	2	3	4
Depth (m)		0 to 0.5	0.5 to 1	1 to 1.5	Below 1.5
Material type		SILT to Sandy SILT	SILT	SILT	Sandy SILT
Unsaturated unit weight, γ_{unsat} (kN/m^3)		17.4	17.4	19.1	20.2
Saturated unit weight, γ_{sat} (kN/m^3)		18.4	18.4	20.1	21.2
Elastic modulus, *E'* (MPa)		6	7	7	7
Poisson's ratio, *v'*		0.35	0.35	0.35	0.35
Effective cohesion, *c'* (kPa)		3	3	3	3
Effective angle of shearing resistance, ϕ'		36°	36°	36°	36°
Saturated permeability, k_{sat} (m/s)		5.8×10^{-7}	2.7×10^{-7}	2.6×10^{-7}	2.4×10^{-7}
VG model fitting parameters (Wetting SWRC)	α (1/m)	0.272	0.226	0.14	
	n	1.315	1.405	1.405	
	m	0.239	0.288	0.288	

VG model fitting parameters (Drying SWRC)	α (1/m)	0.121	0.063	0.063
	n	1.372	1.65	1.65
	m	0.240	0.394	0.394

7.3 Boundary conditions

On both slope models shown in Fig. 7a and b, standard fixities were applied, which allowed vertical movement of the two lateral boundaries, free movement of the upper boundary and restrained movement of the bottom boundary. The hydraulic boundaries at the two lateral sides of the model were set to be closed and the bottom boundary was assigned as an open boundary. On the upper model boundaries, a downward positive flux was prescribed to model infiltration, the input values of which are the actual rainfall amounts specified in the unit of length per unit of time. Similarly, to simulate evapotranspiration during the periods with zero rainfall, on the upper model boundaries, an upward negative flux of 0.167×10^{-3} m/hr or 4 mm/day was applied based on the study by Lambert and Chitrakar (1989).

For the model calibration, the hourly rainfall from 1 July 2019 and 11 July 2019 recorded at the monitoring station was applied as the positive influx. For the analysis of slope stability before the Kanglang landslide failure, due to lack of access to continuous hourly records, daily rainfall from 1 December 2017 to 30 June 2018 measured at the four nearest rainfall stations located between ~6 and 27 km from the study site was obtained from the Department of Hydrology and Meteorology, Nepal (DHM, 2018). Based on these distances, a weighted mean daily rainfall was estimated and prescribed as influx. The back-analysis of the Kanglang landslide and the stability analysis without the road cut were conducted under the July 2018 hourly rainfall recorded at Bahrabise located approximately 11 km south of the study site.

The infiltration amount varies with time and depends on the infiltration capacity of the soil, which is governed largely by the permeability function shown in Eq. (5) (Galavi, 2010). In PLAXIS, if the rainfall intensity is greater than this capacity, ponding occurs at the surface at a prescribed depth of ψ_{max}, which is the water head above the ground surface. If this is exceeded, runoff is simulated. For simplicity, it was assumed that ponding does not occur on sloping ground; hence a small value of maximum pore water pressure head (ψ_{max}) of 0.1 mm was assigned on the upper surface boundaries. To prevent unrealistic suction development due to evapotranspiration, a minimum pressure head (ψ_{min}) of -30 m was prescribed

at the upper surface boundaries. This value corresponds to the minimum volumetric water content of 0.23 m^3/m^3 recorded at 0.3 m depth during a year-long monitoring period from 27 March 2019 to 28 March 2020.

7.4 Initial conditions

The initial stresses were generated using the gravity loading function in PLAXIS, which is recommended for sloping ground (Brinkgreve et al., 2018). With this loading function, PLAXIS generates initial stresses by the application of soil self-weight. The groundwater table was assumed to be 15 m below the upper model boundary as shown in Fig. 7a and b. The initial pore water pressures were generated by applying a constant influx of 3.3×10^{-8} m/s at the ground surface for five years until a steady-state condition was attained where no further change in the pore water pressure with time was observed. After a steady-state condition was reached, actual rainfall was applied as a downward positive influx and an upward negative flux was applied to simulate evapotranspiration at the ground surface.

8. Results

8.1 Model calibration

The calibration results presented in Fig. 8a, b and c illustrate the comparisons between the predicted and measured hourly volumetric water content changes. Since PLAXIS does not produce direct output as volumetric water content, the soil suction predicted by PLAXIS from the fully coupled analysis was converted to volumetric water content using the wetting SWRC. Fig. 8a and b show that at 0.3 and 0.8 m depths, the model predicted a slightly higher increase in volumetric water content during rainfall. At 0.3 m, the starting volumetric water content in the model was ~ 0.01 m^3/m^3 higher than that in the field. At 1.2 m depth, the predicted volumetric water content was found to be in close agreement with the field measurement, as shown in Fig. 8c. The discrepancies between model prediction and field measurement may have resulted from soil heterogeneity, the use of a single wetting SWRC to convert the predicted suction to volumetric water content and hydraulic hysteresis that was not incorporated in PLAXIS. Nonetheless, it is evident that the model effectively captured the overall trend of the volumetric water content changes at all depths. The model also accurately predicted the timing of the increase and decrease

of volumetric water content at the start and end of a rainfall event. Hence, despite some discrepancies in the magnitude of the changes, given the ability of the model to closely capture the hydrologic changes in the field during this monsoonal period of the year, the calibrated model is considered suitable for the subsequent analyses.

(a)

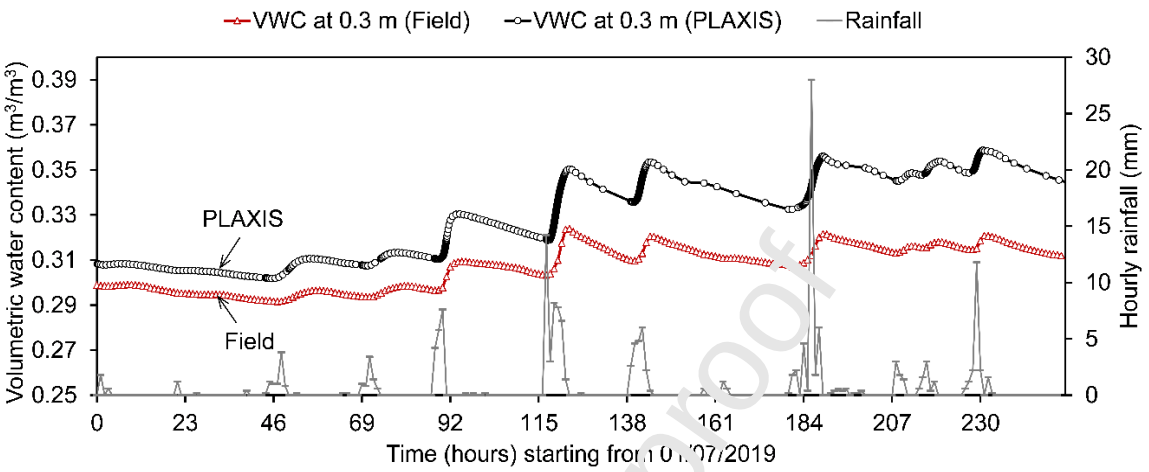

(b)

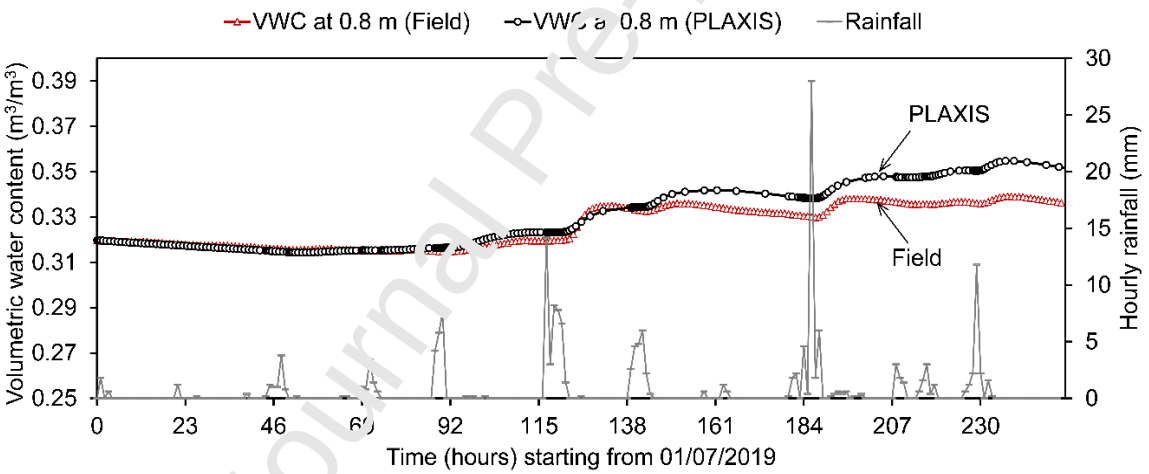

(c)

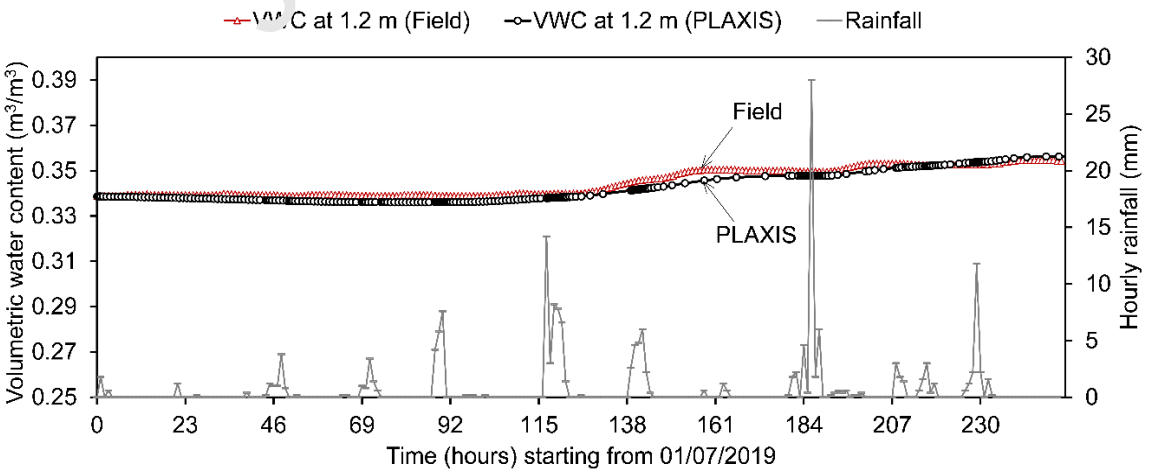

Fig. 8 Model calibration results: comparison between measured average hourly volumetric water content and model predictions from 1 July 2019 00:00 to 11 July 2019 11:00 at (a) 0.3 m (b) 0.8 m and (c) 1.2 m.

8.2 Slope stability analysis before the Kanglang landslide

Fig. 9a and b present the results of the slope stability assessment before the Kanglang landslide from 1 December 2017 (when the slope was excavated) to 30 June 2018 (before the main landsliding event in July 2018). Fig. 9a shows that the changes in the factor of safety during this period are related directly to the wet and dry phases; the wet phases being the days with non-zero rainfall. During the relatively dry period before 28 February 2018, the factor of safety increased to ~3.5. As the wetting SWRC was introduced into the model on 1 March 2018, the factor of safety dropped slightly but remained consistently high until 18 May 2018 when the daily rainfall was 12 mm or less. After 18 May 2018, the factor of safety decreased gradually with the increase in the occurrence of wet phases.

The decrease in the factor of safety shown in Fig. 9a due to the rainfall can be explained in terms of the changes in the effective degree of saturation and relative permeability. Fig. 9b shows that the smaller changes in the factor of safety during the dry period were because of the decreasing effective saturation and relative permeability of the soil so that rainfall infiltration is limited. With the increase in rainfall after 18 May 2018, both the effective degree of saturation and relative permeability increased gradually (Fig. 9b), allowing a greater amount of water to infiltrate into the ground and consequently leading to a drop in the factor of safety. During a few days in June 2018, the factor of safety dropped slightly below 1 but can be seen to recover after a reduction in rainfall. Although this indicates failure conditions were met, it should be noted that variations in rainfall over small distances, such as that between the site and the most local weather station may be significant here. Further, analysis using daily rainfall allows the degree of saturation of soil to rise continuously during consecutive wet days as dry periods during days considered here as 'wet' (e.g., hours) are not taken into consideration. Hence, the factor of safety predicted from this analysis is considered a conservative estimate. Taking this into consideration, it was assumed that the slope was in a stable condition from December 2017 until the end of June 2018.

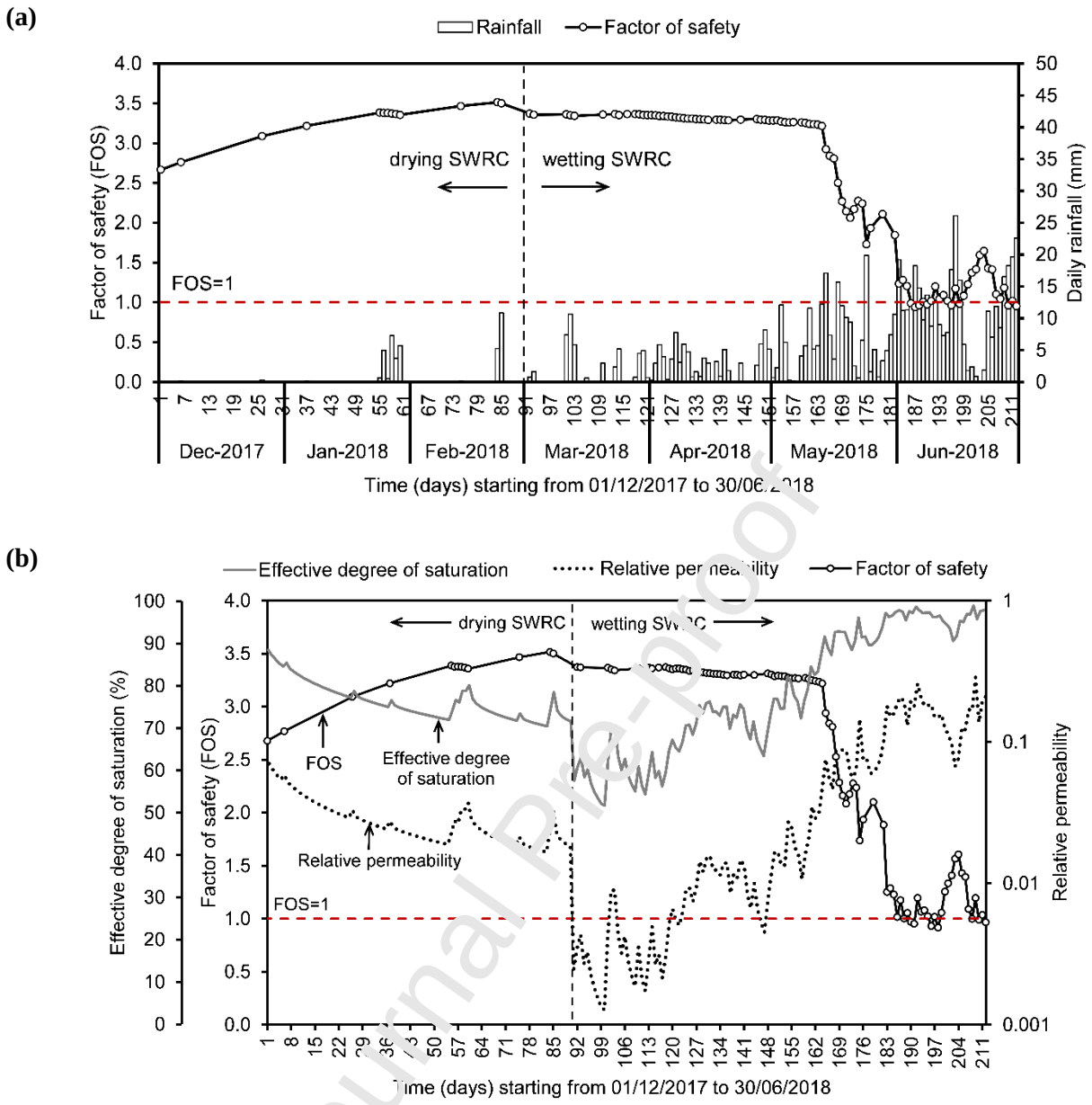

Fig. 9 Daily variations in (a) rainfall and factor of safety from 1 December 2017 to 30 June 2018, and (b) factor of safety, effective degree of saturation and relative permeability from 1 December 2017 to 30 June 2018.

8.3 Back-analysis of the Kanglang landslide

8.3.1 Factor of safety

The solid line in Fig. 10 shows the results of the back-analysis in terms of factor of safety changes in response to rainfall from 1 July to 12 July 2018 (271 hours). Six major rainfall events accumulating >5 mm rainfall were recorded, whose effects on the factor of safety are evident in Fig. 10. Before the 6th rainfall event between 11 and 12 July 2018, the factor of safety that decreased during rainfall can be seen

to recover, although not fully, during the intervening dry periods. During the 6th rainfall event, however, the factor of safety decreased rapidly from 1.2 at 262nd hour (11 July 2018) to 0.97 at 267th hour (12 July 2018) and thereafter remained consistently below 1. This shows that the 6th rainfall event that had a low intensity (4.4 mm/hr) and long duration (10 hours) may have triggered the Kanglang landslide on 12 July 2018. Although the exact time of the actual landslide is not known, this time frame is in line with the landowner's testimony, which confirms that the developed hydro-mechanical model is capable of predicting the time of slope failure.

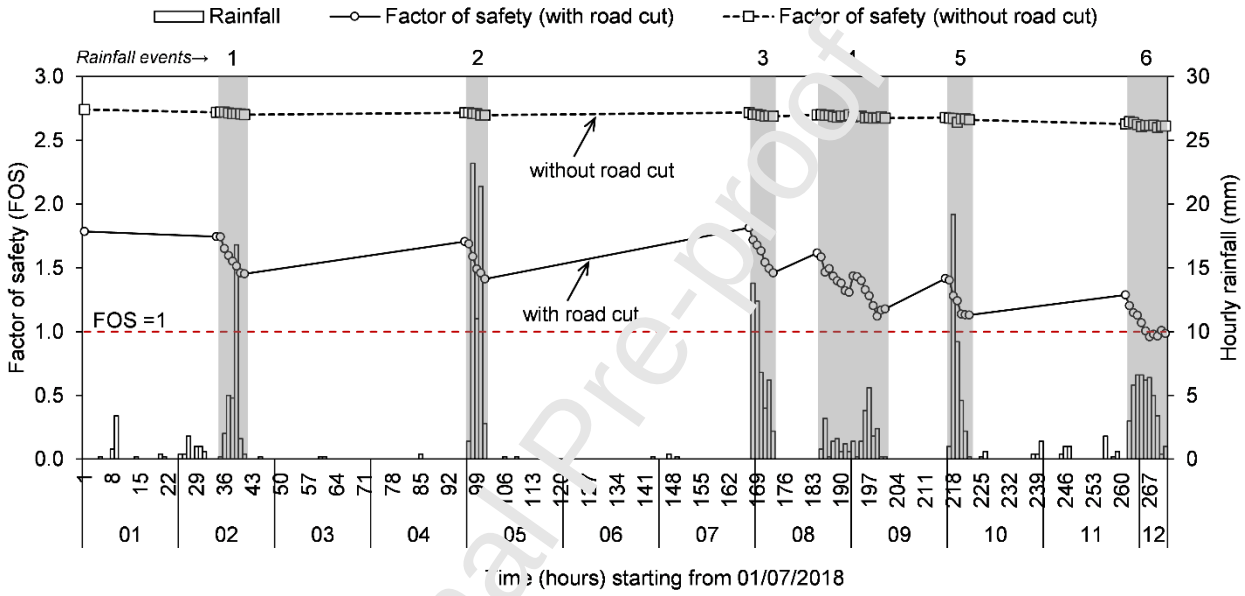

Fig. 10 Hourly variations in factor of safety from 1 July 2018 00:00 to 12 July 2018 06:00. The shaded areas represent major rainfall events accumulating at least 5 mm rainfall.

8.3.2 Soil suction and total displacements

The reductions in the factor of safety during the six rainfall events illustrated in Fig. 10 show the effect of the advancing wetting front on the overall stability of the slope. To better understand the failure mechanism, the effect of rainfall infiltration on the soil suction and total displacements were evaluated.

Fig. 11a and b show the changes in suction at sections A-A* and B-B* (Fig. 11c) during the 6th rainfall event from 261 to 271 hours which was predicted to have triggered the Kanglang landslide (Fig. 10). Indicated by the reduction of suction with increasing cumulative rainfall, these figures reveal the gradual advancement of the wetting front near the road cut (A-A*) and mid-slope (B-B*) sections. On 12 July 2018, when the factor of safety dropped to <1 (267th hour), the wetting front advanced to ~1.3 and 1.1

m at sections A-A* and B-B* respectively. A uniform reduction of suction that is more prominent near the ground surface can also be seen in the suction contours at the time of failure (Fig. 11c). With further infiltration thereafter, the wetting front progressed to ~1.7 and 1.6 m depths at sections A-A* and B-B* respectively.

The advancing wetting front also resulted in increased slope displacements, as illustrated in Fig. 12a, where the direct association between rainfall and displacement can be seen in the three sections within the slope, near the road cut (C-C*), mid-slope (D-D*) and slope crest (E-E*) (Fig. 12c). Near the road cut (C-C*), larger displacements were predicted at shallow depths (≤1.3 m), which corresponds to the depth of the wetting front at this section (~1.3 m) at the time of failure (Fig. 11a and Fig. 12a). Similarly, near the mid-slope section (D-D*) and slope crest (E-E*), larger displacements were predicted at ≤1.3 m, also corresponding to the wetting front depth of ~1.1 m when the failure occurred (Fig. 11b and Fig. 12a). Both the maximum wetting front depths (~1.1 to 1.3 m) and the depths at which larger displacements were predicted by the model (≤1.3 m) are close to the sliding depth of ~1.5 m estimated at the site during field investigation (section 2), which further validates the model prediction.

Further, relatively larger total displacements were predicted closer to the road cut compared to the other sections of the slope and the total displacements can be seen to increase non-linearly with increasing proximity to the road cut (Fig. 12c). The displacement at this section was predicted to increase to 221, 217 and 193 mm at 0, 0.3 m and 0.8 m depths with continued infiltration after the failure, although suction at these depths had not fully dissipated (Fig. 11a and Fig. 12b). Such large displacements despite the presence of suction suggest that the landslide was not triggered alone by the infiltration-induced loss of shear strength. Instead, the landslide was induced by a combined rainfall-road effect, where the rainfall infiltration created a weaker zone with low suction at shallow depths of ≤1.7 m above the road cut, and the presence of the steep road cut promoted the failure by allowing the upslope soil mass to slide, resulting in large displacements at the road cut. Similar results were also reported by Guadagno et al. (2003) where the authors found that the presence of discontinuities in the hillslopes created by road cuts promoted shallow landslides by imparting kinematic freedom to the upslope materials. The results of this study are also in line with the study by Holcombe et al. (2016), where the authors revealed that the slope cuttings in the

hillslope can shift the failure surface towards the face of the cut, ultimately decreasing the factor of safety and causing slope failures.

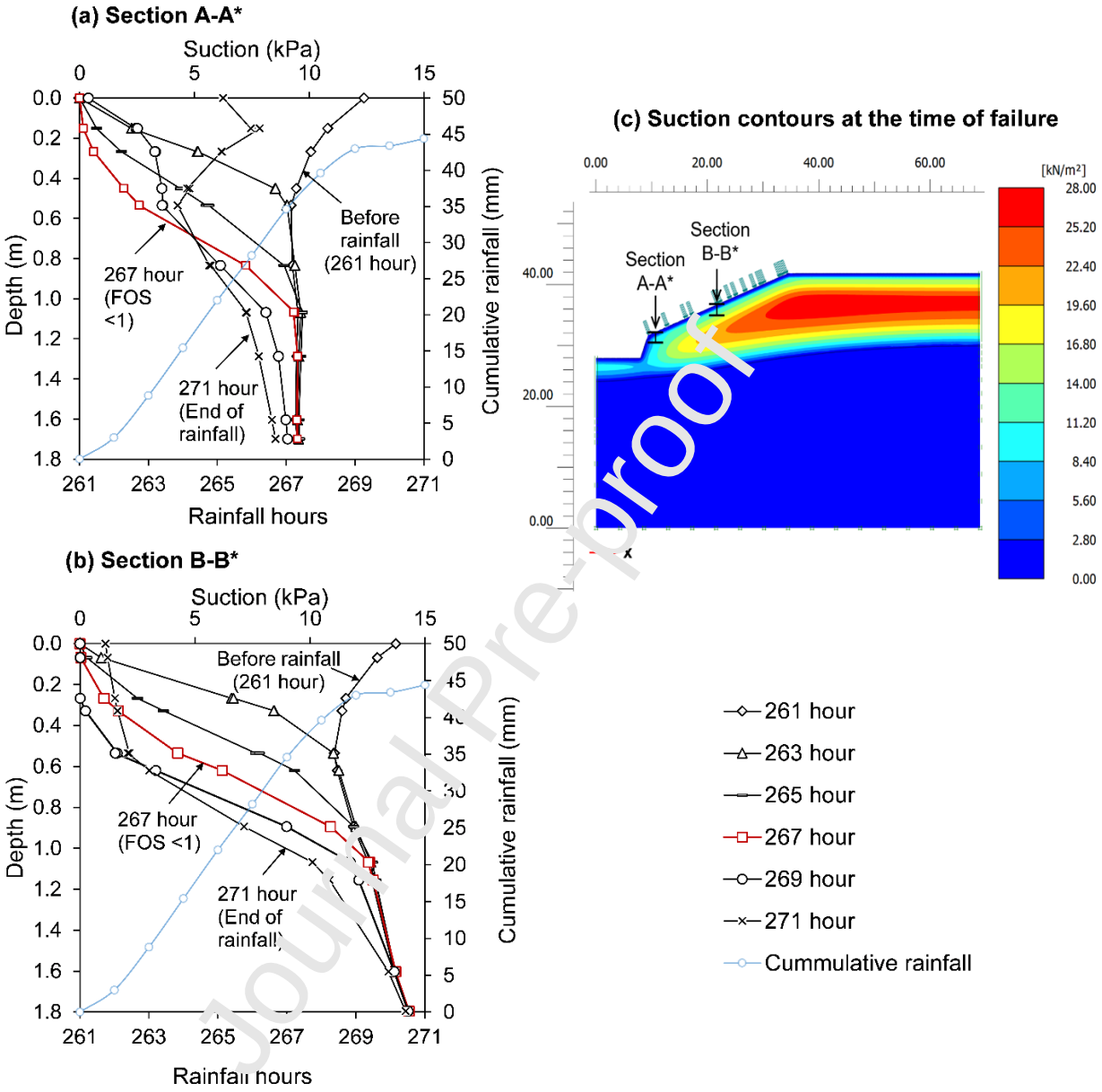

Fig. 11 Variations in soil suction with depth during the 6th rainfall event (from 261 to 271 hours, Fig. x) at (a) section A-A*, (b) section B-B*, and (c) suction contours at the time of failure (267th hour) showing the locations of sections A-A* and B-B*; the vertical and horizontal axes show model dimensions in metres.

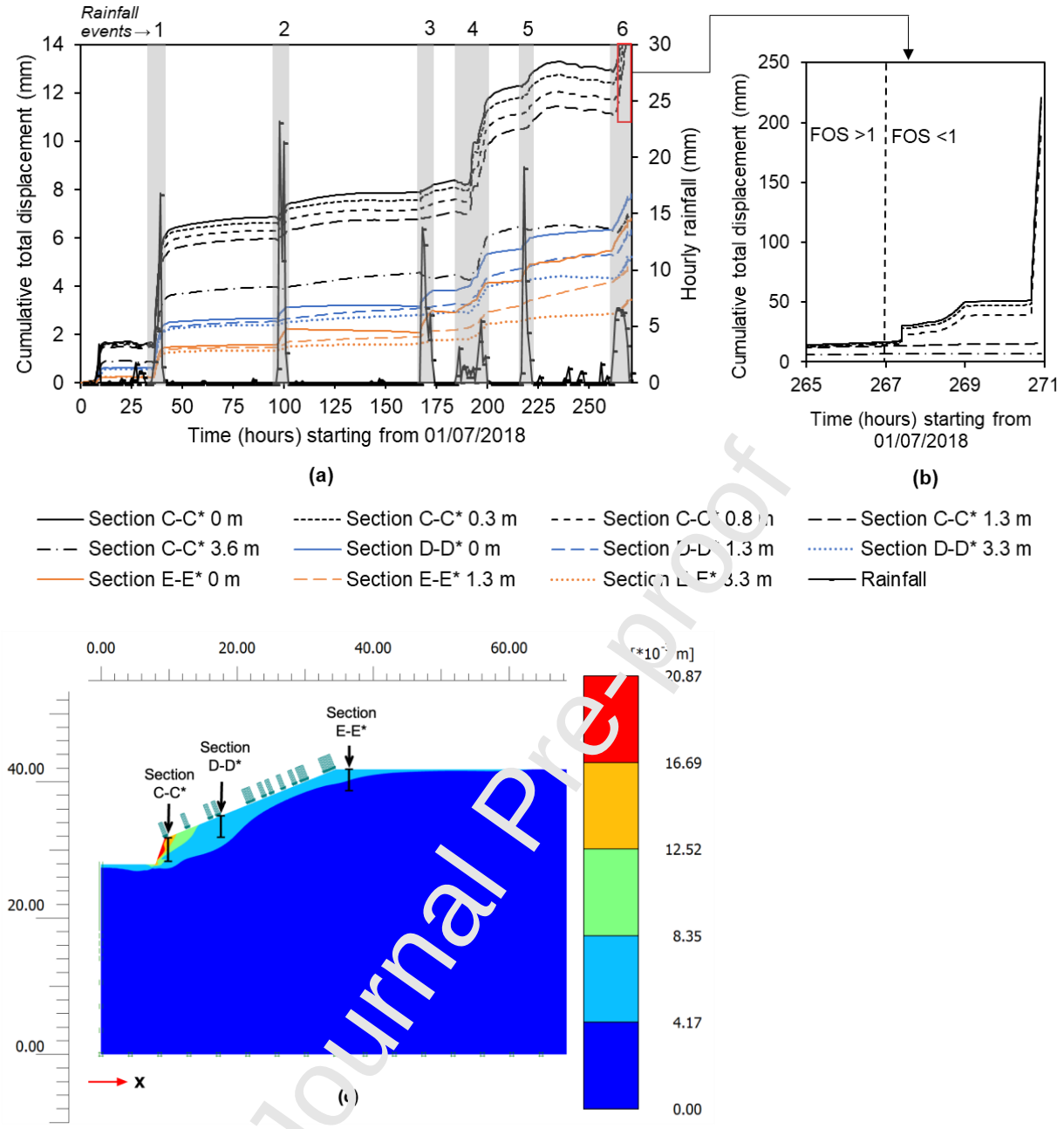

Fig. 12 (a) Hourly rainfall and cumulative total displacements from 1 July 2018 00:00 to 12 July 2018 06:00 measured near the cut slope (section C-C*), mid-slope (section D-D*), and slope crest (section E-E*), (b) increased cumulative total displacements at section C-C* and (c) total displacement contours at the time of failure (267th hour) showing the locations of sections C-C*, D-D*, and E-E*; the vertical and horizontal axes show model dimensions in metres.

8.4 Stability analysis without road cut

To reinforce the back-analysis results, which showed that the presence of the steep road cut promoted the landslide during rainfall, the back-analysis was replicated on a finite element model without the road cut (Fig. 7b), and the results in terms of factor of safety are shown by the dashed line in Fig. 10. The

comparison of the two plots in Fig. 10 clearly illustrates the effect of the road cut on slope stability. The actual slope with the road cut had a ~35% lesser initial factor of safety than that for the idealised, undisturbed slope without the road cut. The presence and absence of the road cut can also be seen to influence the temporal fluctuations of the factor of safety in response to the same series of rainfall events. The model without the road cut remained stable with a factor of safety close to 2.6, while in the actual slope with the road cut, the factor of safety decreased during each rainfall event before eventually dropping below 1 on 12 July 2018. At the time of failure, in comparison to the actual slope, the factor of safety of the undisturbed slope without the road cut was ~170% greater. This suggests that the rainfall events that occurred before, during and after the Kanglang landslide were not sufficiently high to initiate failure in the natural or undisturbed hillslope.

These observations underline two key points: first, the informal modification of the natural hillslopes for road construction, creating steep road cuts, lowers the initial factor of safety by more than 30%, which increases the likelihood of slope failure when exposed to rainfall. Second, the observation that the undisturbed slope remained stable with ~170% higher factor of safety than the actual slope, under the same landslide-triggering rainfall events, shows that the presence of a steep road cut can lower the minimum level of rainfall needed to initiate shallow slope failure, which further aggravates the landslide susceptibility.

8.5 Relationship between rainfall duration and factor of safety

The back-analysis result illustrated in Fig. 10 shows that a relatively greater reduction of the factor of safety was observed during longer duration rainfall events compared to that during shorter duration rainfall events. This result was used to explore the relationship between the rainfall duration and the corresponding change in the factor of safety. A statistically significant correlation (R^2=0.97, $p<0.001$) was obtained (Fig. 13), which suggests that an increase in rainfall duration from 5 to 17 hours could cause an additional ~10% drop in the factor of safety. While the correlation is based on a limited dataset, the relationship between the two variables suggests that a greater decline in the factor of safety can be expected during long-duration rainfall events compared to during shorter duration rainfall events. This observation agrees with the study by Rahardjo et al. (2007) where the authors showed that slopes with low saturated permeability ($\leq 10^{-6}$ m/s) are less affected by short-duration rainfall events, regardless of the

rainfall intensity. Such a response can be explained in terms of the infiltration-permeability ratio (I_r/k_{sat}) as discussed by Tsaparas et al. (2002). In soils with low permeability, during high-intensity, short-duration rainfall events (high I_r/k_{sat} ratio), less water can infiltrate into the ground, resulting in smaller changes to the factor of safety. On the other hand, when this ratio is smaller, as would be the case for low-intensity, longer duration rainfall events, a greater amount of water can infiltrate into the soil and influence the stability of the slope, resulting in a greater decrease in the factor of safety. As rainfall duration plays a critical role in the slopes with low saturated permeability, high-intensity, long-duration rainfall events may be able to cause a relatively greater decrease in the factor of safety than the low-intensity, long-duration rainfall events. However, this may also be controlled by the infiltration capacity of the soil, which partially depends on the initial conditions of the slope (Tsaparas et al., 2002).

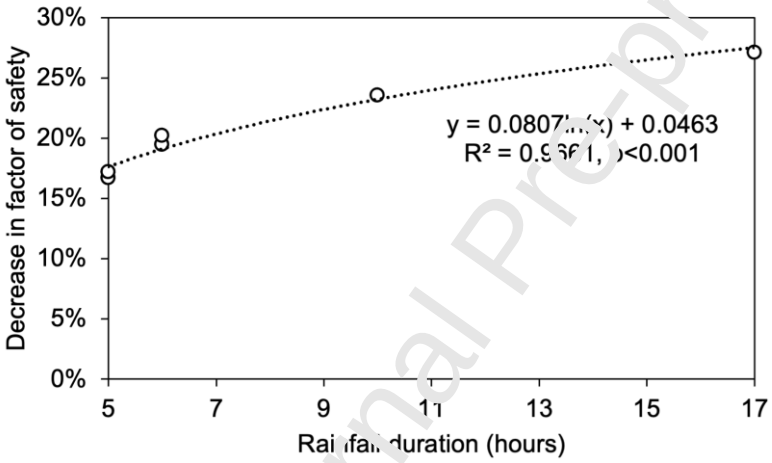

Fig. 13 Relationship between rainfall duration and consequent decrease in factor of safety from 1 July 2018 00:00 to 12 July 2018 06:00

9. Discussion

In low- and middle-income countries like Nepal, roads are considered fundamental infrastructures, expected to contribute to the socio-economic development of local communities. When the poorly constructed roads become one of the landslide causative factors, the consequences present a contradiction to the primary objective of building the roads. In other developing parts of the world besides Nepal, hillslope excavation for roads or for creating flatter sites for urbanisation has also been associated with significant landslide and erosion problems (Haigh and Rawat, 2012; Holcombe et al., 2016; Sidle and Ochiai, 2006; Sidle and Ziegler, 2012). While the road networks continue to proliferate across many

countries to meet the developmental goals, the need to acknowledge and address the adverse impacts of poorly constructed roads becomes more necessary than ever.

Using a case study of a typical landslide that occurred following a non-engineered slope excavation, the numerical analyses presented in this paper demonstrate how such activities can contribute to landsliding during rainfall. The back-analysis of the investigated landslide showed that when the failure occurred in July 2018, the rainfall infiltration in the unsaturated ground caused a gradual reduction of soil suction at shallow depths (≤1.7 m), but not to a point where the suction dissipated completely or positive pore water pressures started to build up. Despite this, the landslide occurred, which to a large extent, was promoted by the presence of the road cut that allowed the weaker upslope materials with low suctions to slide, resulting in large displacements at the road cut.

Although the consequences of steep slope cutting for road construction on the occurrence of rainfall-induced landslides are generally well understood and there are both supporting anecdotal and statistical evidence, the results of this study provide a valuable reference that quantifies this effect. More specifically, results show that the presence of a steep road cut on a natural hillslope could reduce the initial factor of safety by ~35%, thereby increasing the susceptibility to landsliding during rainfall. Further, the stability of the undisturbed hillslope (without road cut) under the same rainfall conditions that triggered the investigated landslide (with road cut) clearly shows that the presence of a single road cut can lower the level of minimum rainfall needed to initiate slope failure. It is critical to recognise that a significant proportion of landslides in Nepal occurs during the monsoon when almost 80% of the annual rainfall is expected to occur. The lowering of the minimum landslide-triggering rainfall for slopes modified by road construction means that the rainfall-induced roadside slope failures will become more frequent and extensive during the monsoon if the hillslopes continue to be informally excavated without suitable engineering interventions. The proposed empirical relationship between rainfall duration and percentage decrease in factor of safety further suggests that the reduction of the factor of safety or the risk of slope failure is greater during longer duration rainfall events in modified natural hillslopes with similar soil properties as was encountered at the investigated site. The relevance of the findings of this study extends beyond the presented case study to other developing regions globally, where the road infrastructures need to be better planned and constructed, with a particular focus on minimising the risk of slope instabilities

that have both short- and long-term cumulative impacts on the lives, infrastructures and the environment in general.

Where economic constraints prevent the adoption of engineering design-based slope protection measures, cost-effective retaining structures such as dry stone and mortared masonry walls, gabion walls and crib walls that utilise locally available materials, can help prevent or mitigate roadside slope failures during rainfall (Hearn, 2011). Bio-engineering techniques such as plantation of deep-rooted plant species, turfing and jute netting are other cost-effective slope protection measures (Devkota et al., 2014). Constructing gentler roadside slopes with angles lower than the angle of shearing resistance of the soil, while adhering to the road construction guidelines e.g. DoR (2003), TRL (1997) is another simple approach that can help prevent rainfall-induced roadside slope failures.

On the slopes that have a high landslide potential during rainfall and pose a greater risk to lives and infrastructures, landslide prediction can prevent disasters from occurring. This study demonstrates the abilities of the coupled hydro-mechanical analysis, with Bishop's effective stress and single wetting SWRC to simulate the long-term hydrological changes in the unsaturated soils and most importantly, to predict the failure timing and failure mechanism of slopes under transient wetting and drying conditions. Application of this approach requires comprehensive site-specific field study, laboratory testing of (un)saturated soil properties and meteorological data, acquiring which may not be feasible in all conditions. This also underlines the need for quality geotechnical and meteorological data in developing countries for the prediction, prevention and mitigation of rainfall-induced landslides. Nonetheless, the lack of geotechnical data could be tackled by obtaining information through empirical estimations, published scientific literature or by utilising community knowledge and participation, as employed by Anderson and Holcombe (2013).

10. Conclusions

This paper presented a case study of a typical roadside slope failure (Kanglang landslide) located in Sindhupalchok district in Nepal that was triggered by the monsoon rainfall in July 2018. An integrated approach combining detailed field investigation, laboratory testing, field monitoring and coupled flow-deformation analyses in PLAXIS 2D was used to understand the failure mechanism of the landslide and to

assess the role of rainfall and road cut in inducing this failure. From the work presented in this study, the following conclusions can be drawn:

1. The back-analysis results showed that the Kanglang landslide occurred during a low intensity (4.4 mm/hr), long duration (10 hours) rainfall event on 12 July 2018, which agrees with the landowner's testimony that the failure occurred before 16 July 2018. The landslide was caused by a combined effect of rainfall and road cut where the infiltration of rainwater created a weaker zone with low suction at shallow depths of (≤1.7 m) and the presence of the road cut promoted the failure by allowing the upslope materials to slide, resulting in large displacements of ~200 mm at the road cut.
2. Comparison between the two slope models representing the actual slope (with the road cut) and the idealised undisturbed slope (without the road) showed that the presence of a single steep road cut can increase the susceptibility of slope failure in two ways: first, by reducing the initial factor of safety by over 30%; and second, by lowering the minimum level of rainfall needed to initiate slope failure. This implies that the rainfall-induced roadside slope failures will become more frequent and extensive in the future if the slopes continue to be informally excavated for constructing roads or for other developmental activities.
3. A statistically significant correlation was found between rainfall duration and percentage decrease in the factor of safety. This relationship suggested that in the informally excavated steep road cut slopes underlain by lower permeability SILTS and Sandy SILTS, as encountered at the investigated site, a greater reduction of the factor of safety can be expected during longer duration rainfall events; an increase in the rainfall duration from 5 to 17 hours could cause an additional ~10% decrease in the factor of safety.
4. Using the measured soil properties, site geometry and rainfall records, this study demonstrated the viability of the coupled-hydromechanical analysis to effectively capture the hydrologic changes in the soil in response to transient atmospheric conditions, and most importantly, to predict the timing of slope failure and to assess the failure mechanism of rainfall-induced slope failure. For slopes with high rainfall-induced landslide susceptibility that pose a serious risk to lives and infrastructures, landslide prediction using this approach can prevent disasters from occurring. Where hydraulic hysteresis cannot be taken into consideration in the hydro-mechanical analysis, this study also

showed that the wetting soil water retention curve can be suitably adopted to model the hydraulic behaviour of unsaturated soils.

The results from this study provide a reference for recognising the detrimental impact of informal slope cutting for road construction on the occurrence of rainfall-induced landsliding. This should be taken into consideration in future disaster mitigation and reduction strategies in areas where increasing rural access through road construction is also a priority.

Acknowledgement

This research was supported by the Institute of Hazard, Risk and Resilience (IHRR), Durham University, UK under the Action on Natural Disasters (AND) doctoral training initiative.

AUTHOR'S STATEMENT

Samprada Pradhan: Conceptualisation, Methodology, Software, Validation, Formal Analysis, Investigation, Writing – Original Draft, Visualisation. **David G. Toll, Nick Rosser, Matthew J. Brain:** Conceptualisation, Resources, Writing - Review and Editing, Supervision.

Declaration of interests

The authors declare that they have no known competing financial interests or personal relationships that could have appeared to influence the work reported in this paper.

The authors declare the following financial interests/personal relationships which may be considered as potential competing interests

References

Alonso, E.E., Pereira, J.M., Vaunat, J., Olivella, S., 2010. A microstructurally based effective stress for unsaturated soils. Geotechnique 60, 913–925. https://doi.org/10.1680/geot.8.P.002

Anderson, M., Holcombe, E., 2013. Community-based landslide risk reduction. https://doi.org/10.1596/978-0-8213-9456-4

Bentley Systems Inc., 2018. https://www.bentley.com/en/products/brands/plaxis [WWW Document].

Biot, M.A., 1941. General theory of three-dimensional consolidation. J. Appl. Phys. 12, 155–164.

Bishop, A.W., 1959. The principle of effective stress. Tek. Ukebl. 39, 859–863.

Bishop, A.W., Blight, G.E., 1963. Some aspects of effective stress in saturated and partly saturated soils. Geotechnique 13, 177–197. https://doi.org/10.1680/geot.1963.13.3.177

Bowles, J.E., 1997. Foundation analysis and design, 5th ed. The McGraw-Hill Companies, Inc.

Brand, E.W., 1981. Some thoughts on rain-induced slope failures. Soil Mech. Found. Eng. Proc. 10th Int. Conf. Stock. June 1981. Vol. 3, 372–376.

Brinkgreve, R.B.J., Kumarswamy, S., Swolfs, W.M., Foria, F., 2018. PLAXIS 2D reference manual 2018.

BSI, 2019. Geotechnical investigation and testing - Laboratory testing of soil - Part 11: Permeability tests (BS EN ISO 17892-11:2019).

BSI, 2018a. Geotechnical investigation and testing - Laboratory testing of soil - Part 12: Determination of liquid and plastic limits (BS EN ISO 17892-12:2018).

BSI, 2018b. Geotechnical investigation and testing - Laboratory testing of soil - Part 9: Consolidated triaxial compression tests on water saturated soils (BS EN ISO 17892-9:2018).

BSI, 2017. Soil quality - Sampling - Part 102: Selection and application of sampling techniques (BS ISO 18400-102:2017).

BSI, 2015. Code of practice for ground investigations (BS 5930:2015).

BSI, 2005. Geotechnical investigation and testing - Field testing - Part 3: Standard penetration test (BS EN ISO 22476-3:2005+A1:2011).

Cai, F., Ugai, K., 2004. Numerical analysis of rainfall effects on slope stability. Int. J. Geomech. 4, 69–78. https://doi.org/10.1061/(ASCE)1532-3641(2004)4:2(69)

Casini, F., Minder, P., Springman, S.M., 2011. Shear strength of an unsaturated silty sand. Unsaturated Soils - Proc. 5th Int. Conf. Unsaturated Soils 1, 211–216. https://doi.org/10.1201/b10526-24

Chen, P., Lu, N., Formetta, G., Godt, J.W., Wayllace, A., 2018. Tropical storm-induced landslide potential using combined field monitoring and numerical modeling. J. Geotech. Geoenvironmental Eng. 144. https://doi.org/10.1061/(asce)gt.1943-5606.0001969

Collison, A.J.C., Anderson, M.G., Lloyd, D.M., 1995. Impact of vegetation on slope stability in a humid tropical environment: A modelling approach. Proc. Inst. Civ. Eng. Water, Marit. Energy 112, 168–175. https://doi.org/10.1680/iwtme.1995.27662

Dahal, R.K., Hasegawa, S., 2008. Representative rainfall thresholds for landslides in the Nepal Himalaya. Geomorphology 100, 429–443. https://doi.org/https://doi.org/10.1016/j.geomorph.2008.01.014

Dahal, R.K.R., Hasegawa, S., Bhandary, N.P., Yatabe, R., 2010. Low cost road for the development of Nepal and its engineering geological consequences, in: Williams, A.L., Pinches, G.M., Chin, C.Y., McMorran, T.J., Massey, C.I. (Eds.), Proceedings of the 11th IAEG Congress. Taylor & Francis Group, London, Auckland, pp. 4085–4094.

Devkota, S., Sudmeier-Rieux, K., Penna, I., Erble, S., Jaboyedoff, M., Andhikari, A., Khanal, R., 2014. Community-based bio-engineering for eco-safe roadsides in Nepal.

DHM, 2018. Precipitation data.

Dixit, A., Neupane, S., Bhandari, D., Aacharya, B.K., 2021. Political economy of 2020 landslides, road construction and disaster risk reduction in Nepal. Nepal.

Dixon, N., Crosby, C.J., Stirling, R., Hughes, P.N., Smethurst, J., Briggs, K., Hughes, D., Gunn, D., Hobbs, P., Loveridge, F., Glendinning, S., Dijkstra, T., Hudson, A., 2019. In situ measurements of near-surface hydraulic conductivity in engineered clay slopes. Q. J. Eng. Geol. Hydrogeol. 52, 123–135. https://doi.org/10.1144/qjegh2017-059

DMG, 1994. Geology of Nepal. Department of Mines and Geology, ICIMOD, Nepal.

DoR, 2003. Guide to road slope protection works. Government of Nepal; Ministry of Physical Planning and Works; Department of Roads (DoR), Kathmandu, Nepal.

Fredlund, D.G., 1987. Slope stability analysis incorporating the effect of soil suction, in: Anderson, M.G., Richards, K.S. (Eds.), Slope Stability. John Wiley & Sons, Ltd, pp. 113–144.

Fredlund, D.G., Morgenstern, N.R., Widger, R.A., 1978. The shear strength of unsaturated soils. Can. Geotech. J. 15, 313–321. https://doi.org/10.1139/t78-029

Fredlund, D.G., Rahardjo, H., 1993. The role of unsaturated soil behaviour in geotechnical engineering practice. 11th Southeast Asian Geotech. Conf.

Froude, M.J., Petley, D.N., 2018. Global fatal landslide occurrence from 2004 to 2016. Nat. Hazards Earth Syst. Sci. 18, 2161–2181. https://doi.org/10.5194/nhess-18-2161-2018

Galavi, V., 2010. Groundwater flow, fully coupled flow deformation and undrained analyses in PLAXIS 2D and 3D. https://doi.org/10.13140/RG.2.1.1940.7763

Galavi, V., Brinkgreve, R.B.J., Bonnier, P.G., Gonzalez, N.A., 2009. Fully coupled hydro-mechanical analysis of unsaturated soils, in: Pietruszczak, S., Pande, G.N., Tamagnini, C., Wan, R. (Eds.), Proceedings of the 1st International Symposium on Computational Geomechanics (COMGEO I). Paris, France.

Gasmo, J.M., Rahardjo, H., Leong, E.C., 2000. Infiltration effects on stability of a residual soil slope. Comput. Geotech. 26, 145–165. https://doi.org/10.1016/S0266-352X(99)00035-X

Godt, J.W., Baum, R.L., Lu, N., 2009. Landsliding in partially saturated materials. Geophys. Res. Lett.

36, 1–5. https://doi.org/10.1029/2008GL035996

Griffiths, D. V., Lane, P.A., 1999. Slope stability analysis by finite elements. Géotechnique 49, 387–403. https://doi.org/10.1680/geot.1999.49.3.387

Guadagno, F.M., Martino, S., Mugnozza, G.S., 2003. Influence of man-made cuts on the stability of pyroclastic covers (Campania, southern Italy): a numerical modelling approach. Environ. Geol. 43, 371–384. https://doi.org/10.1007/s00254-002-0658-0

Haigh, M., Rawat, J., 2012. Landslide disasters: seeking causes – A case study from Uttarakhand, India, in: Křeček, J., Haigh, M., Hofer, T., Kubin, E. (Eds.), Management of Mountain Watersheds. Capital Publishing Company, pp. 218–253. https://doi.org/10.1007/978-94-007-2476-1_18

Hamdhan, I.N., Schweiger, H.F., 2013. Finite element method-based analysis of an unsaturated soil slope subjected to rainfall infiltration. Int. J. Geomech. 13, 653–658. https://doi.org/10.1061/(ASCE)GM.1943-5622.0000239

Hatanaka, M., Uchida, A., 1996. Empirical correlation between penetration resistance and internal friction angle of sandy soils. Soils Found. 36, 1–9. https://doi.org/10.3208/sandf.36.4_1

Hearn, G.J., 2011. Slope engineering for mountain roads. Engineering geology special publication. Geological Society of London, London. https://doi.org/https://doi.org/10.1144/EGSP24

Hearn, G.J., Shakya, N.M., 2017. Engineering challenges for sustainable road access in the Himalayas. Q. J. Eng. Geol. Hydrogeol. 2017. https://doi.org/10.1144/qjegh2016-109

Holcombe, E.A., Beesley, M.E.W., Vardanega, P.J., Sorbie, R., 2016. Urbanisation and landslides: hazard drivers and better practices. Proc. Inst. Civ. Eng. - Civ. Eng. 169, 137–144. https://doi.org/10.1680/jcien.15.00044

Jennings, J.E.B., Burland, J.B., 1962. Limitations to the use of effective stresses in partly saturated soils. Geotechnique 12, 125–144. https://doi.org/10.1680/geot.1962.12.2.125

Karki, R., Talchabhadel, R., Aalto, J., Baidya, S.K., 2016. New climatic classification of Nepal. Theor. Appl. Climatol. 125, 799–808. https://doi.org/10.1007/s00704-015-1549-0

Khalili, N., Khabbaz, M.H., 1998. A unique relationship for χ for the determination of the shear strength of unsaturated soils. Geotechnique 48, 681–687. https://doi.org/10.1680/geot.1998.48.5.681

Kim, J., Hwang, W., Kim, Y., 2018. Effects of hysteresis on hydro-mechanical behavior of unsaturated soil. Eng. Geol. 245, 1–9. https://doi.org/10.1016/j.enggeo.2018.08.004

Kincey, M.E., Rosser, N.J., Robinson, T.R., Densmore, A.L., Shrestha, R., Pujara, D.S., Oven, K.J., Williams, J.G., Swirad, Z.M., 2021. Evolution of coseismic and post-seismic landsliding after the 2015 Mw 7.8 Gorkha Earthquake, Nepal. J. Geophys. Res. Earth Surf. 126. https://doi.org/10.1029/2020JF005803

Kristo, C., Rahardjo, H., Satyanaga, A., 2019. Effect of hysteresis on the stability of residual soil slope. Int. Soil Water Conserv. Res. 7, 226–238. https://doi.org/10.1016/j.iswcr.2019.05.003

Laloui, L., Ferrari, A., Li, C., Eichenberger, J., 2016. Hydro-mechanical analysis of volcanic ash slopes during rainfall. Geotechnique 66, 220–231. https://doi.org/10.1680/jgeot.15.LM.001

Lambert, L., Chitrakar, B.D., 1989. Variation of potential evapotranspiration with elevation in Nepal. Mt. Res. Dev. 9, 145–152. https://doi.org/10.2307/3673477

Li, A.G., Tham, L.G., Yue, Z.Q., Lee, C.F., Law, K.T., 2005. Comparison of field and laboratory soil–water characteristic curves. J. Geotech. Geoenvironmental Eng. 131, 1176–1180. https://doi.org/10.1061/(asce)1090-0241(2005)131:9(1176)

Lourenço, S., Gallipoli, D., Toll, D., Evans, F., Medero, G., 2007. Determination of the Soil Water Retention Curve with Tensiometers. Exp. Unsaturated Soil Mech. 95–102. https://doi.org/10.1007/3-540-69873-6_9

Lourenço, S.D.N., Gallipoli, D., Toll, D.G., Evans, F.D., 2006. Development of a commercial tensiometer for triaxial testing of unsaturated soils. Geotech. Spec. Publ. 40802, 1875–1886. https://doi.org/10.1061/40802(189)158

Lu, N., Likos, W.J., 2004. Unsaturated soil mechanics. John Wiley & Sons, Inc., New Jersey, United States of America.

Lumb, P., 1975. Slope failures in Hong Kong. Q. J. Eng. Geol. 8, 31–65. https://doi.org/10.1144/GSL.QJEG.1975.008.01.02

Matsui, T., San, K.-C., 1992. Finite element slope stability analysis by shear strength reduction technique. Soils Found. 32, 59–70. https://doi.org/10.3208/sandf1972.32.59

Mcadoo, B.G., Quak, M., Gnyawali, K., Adhikari, B.R., Devkota, S., Rajbhandari, P., Sudmeier, K., 2018. Brief communication: Roads and landslides in Nepal: How development affects risk. Nat. Hazards Earth Syst. Sci. Discuss. 1–6. https://doi.org/10.5194/nhess-2017-461

Md. Rahim, M.S., 2016. Hydro-mechanical behaviour of a residual soil slope in Malaysia. PhD Thesis. Durham University.

Md. Rahim, M.S., Toll, D., 2014. Fully coupled flow-deformation analyses of infiltration and matric suctions within a tropical soil slope, in: Khalili, N., Russell, A.R., Khoshghalb, A. (Eds.), Unsaturated Soils: Research and Applications. CRC Press/Balkema, Taylor & Francis Group, London, pp. 1453–1458. https://doi.org/https://doi.org/10.1201/9781003070580

Mohan, D., Aggarwal, V.S., Tolia, D.S., 1970. Discussion: The correlation of cone size in the dynamic cone penetration test with the standard penetration test. Géotechnique 20, 315–319. https://doi.org/10.1680/geot.1971.21.4.423

NDRRMA, 2021. BIPAD: Building Information Platform Against Disaster [WWW Document]. Natl.

Disaster Risk Reduct. Manag. Auth. disaster Inf. Manag. Syst. URL https://bipadportal.gov.np/ (accessed 8.14.21).

Öberg, A., Sällfors, G., 1997. Determination of shear strength parameters of unsaturated silts and sands based on the water retention curve. Geotech. Test. J. 20, 40–48. https://doi.org/10.1520/gtj11419j

Oh, S., Lu, N., 2015. Slope stability analysis under unsaturated conditions: Case studies of rainfall-induced failure of cut slopes. Eng. Geol. 184, 96–103. https://doi.org/10.1016/j.enggeo.2014.11.007

ONSET, 2019. HOBO RX3000 Remote monitoring station data logger manual.

ONSET, 2018. Rain gauge smart sensor (S-RGx-M002) manual. 16 June 2020.

Petley, D.N., Hearn, G.J., Hart, A., Rosser, N.J., Dunning, S.A., Oven, K., Mitchell, W.A., 2007. Trends in landslide occurrence in Nepal. Nat. Hazards 43, 23–44. https://doi.org/10.1007/s11069-006-9100-3

Pradhan, S., Toll, D.G., Rosser, N.J., Brain, M.J., 2020. Field monitoring of soil-moisture to understand the hydrological response of a road-cut slope. E3S Web Conf. 195, 01029. https://doi.org/10.1051/e3sconf/202019501029

Qi, S., Vanapalli, S.K., 2015. Hydro-mechanical coupling effect on surficial layer stability of unsaturated expansive soil slopes. Comput. Geotech. 70, 68–82. https://doi.org/10.1016/j.compgeo.2015.07.006

Rahardjo, H., Kim, Y., Satyanaga, A., 2019. Role of unsaturated soil mechanics in geotechnical engineering. Int. J. Geo-Engineering 10, 1–23. https://doi.org/10.1186/s40703-019-0104-8

Rahardjo, H., Ong, T.H., Rezaur, R.B., Leong, E.C., 2007. Factors controlling instability of homogeneous soil slopes under rainfall. Geotech. Geoenvironmental Eng. 133. https://doi.org/10.1061/(ASCE)1090-0241(2007)133:12(1532)

Roback, K., Clark, M.K., West, A.J., Zekkos, D., Li, G., Gallen, S.F., Chamlagain, D., Godt, J.W., 2018. The size, distribution, and mobility of landslides caused by the 2015 Mw7.8 Gorkha earthquake, Nepal. Geomorphology 301, 121–138. https://doi.org/https://doi.org/10.1016/j.geomorph.2017.01.030

Robson, E., Utili, S., Milledge, D., Upadhaya, N., 2021. Road slope stabilisation in Nepal: stakeholder perspectives, in: Cabrera, M.A., Prada-Sarmiento, L.F., Monter, J. (Eds.), 13th International Symposium on Landslides. Cartagena, Colombia.

Rosser, N., Kincey, M., Oven, K., Densmore, A., Robinson, T., Pujara, D.S., Shrestha, R., Smutny, J., Gurung, K., Lama, S., Dhital, M.R., 2021. Changing significance of landslide hazard and risk after the 2015 Mw 7.8 Gorkha, Nepal Earthquake. Prog. Disaster Sci. 10, 100159. https://doi.org/10.1016/j.pdisas.2021.100159

Rouainia, M., Davies, O., OBrien, T., Glendinning, S., 2009. Numerical modelling of climate effects on slope stability. Proc. Inst. Civ. Eng. Bridg. Eng. 162, 81–89.

https://doi.org/10.1680/ensu.2009.162.2.81

Sati, S.P., Sundriyal, Y.P., Rana, N., Dangwal, S., 2011. Recent landslides in Uttarakhand: Nature's fury or human folly. Curr. Sci. 100, 1617–1620.

Sidle, R.C., Furuichi, T., Kono, Y., 2011. Unprecedented rates of landslide and surface erosion along a newly constructed road in Yunnan, China. Nat. Hazards 57, 313–326.

Sidle, R.C., Ghestem, M., Stokes, A., 2014. Epic landslide erosion from mountain roads in Yunnan, China-challenges for sustainable development. Nat. Hazards Earth Syst. Sci. 14, 3093–3104. https://doi.org/10.5194/nhess-14-3093-2014

Sidle, R.C., Ochiai, H., 2006. Landslides: Processes, prediction, and land use, Water Resources Monograph. American Geophysical Union, Washington DC. https://doi.org/10.1029/WM018

Sidle, R.C., Ziegler, A.D., 2012. The dilemma of mountain roads. Nat. Geosci. 5, 437–438. https://doi.org/10.1038/ngeo1512

Skempton, A.W., 1985. Residual strength of clays in landslides, folded strata and the laboratory. Geotechnique 35, 3–18. https://doi.org/10.1680/geot.1985.35.1.3

Song, X., Borja, R.I., 2014. Mathematical framework for unsaturated flow in the finite deformation range. Int. J. Numer. Methods Eng. 97, 658–682. https://doi.org/10.1002/nme.4605

Springman, S.M., Jommi, C., Teysseire, P., 2003. Instabilities on moraine slopes induced by loss of suction: A case history. Geotechnique 53, 3–10. https://doi.org/10.1680/geot.2003.53.1.3

Stöcklin, J., 1980. Geology of Nepal and its regional frame: Thirty-third William Smith Lecture. J. Geol. Soc. London. 137, 1–34.

Tanoli, J.I., Ningsheng, C., Regmi, A.D., Jun, L., 2017. Spatial distribution analysis and susceptibility mapping of landslides triggered before and after Mw7.8 Gorkha earthquake along Upper Bhote Koshi, Nepal. Arab. J. Geosci. 10, 277. https://doi.org/10.1007/s12517-017-3026-9

Tian, Y., Owen, L.A., Xu, C., Ma, S., Li, K., Xu, X., Figueiredo, P.M., Kang, W., Guo, P., Wang, S., Liang, X., Maharjan, S.B., 2020. Landslide development within 3 years after the 2015 Mw 7.8 Gorkha earthquake, Nepal. Landslides 17, 1251–1267. https://doi.org/10.1007/s10346-020-01366-x

Toll, D.G., 2020. Stress components in unsaturated soils. Geotech. Eng. J. SEAGS AGSSEA 51, 19–24.

Toll, D.G., Lourenço, S.D.N., Mendes, J., 2013. Advances in suction measurements using high suction tensiometers. Eng. Geol. 165, 29–37. https://doi.org/10.1016/j.enggeo.2012.04.013

Toll, D.G., Md. Rahim, M.S., Karthikeyan, M., Tsaparas, I., 2019. Soil–atmosphere interactions for analysing slopes in tropical soils in Singapore. Environ. Geotech. 6, 361–372. https://doi.org/10.1680/jenge.15.00071

TRL, 1997. Overseas road note 16: Principles of low cost road engineering in mountainous regions. Berkshire, UK.

Tsaparas, I., Rahardjo, H., Toll, D.., Leong, E.., 2002. Controlling parameters for rainfall-induced landslides. Comput. Geotech. 29, 1–27. https://doi.org/10.1016/S0266-352X(01)00019-2

UNDP, 2011. Economic analysis of local government investment in rural roads in Nepal 2011. Ministry of Local Development;Local Governance and Community Development Programme (LGCDP);United Nations Development Programme (UNDP), Lalitpur, Nepal.

Upreti, B.N., 2001. The physiography and geology of Nepal and their bearing on the landslide problem. Landslide Hazard Mitig. Hindu Kush-Himalayas.

Upreti, B.N., 1996. Stratigraphy of the western Nepal Lesser Himalaya: A synthesis. J. Nepal Geol. Soc. 13, 11–28. https://doi.org/10.3126/jngs.v13i0.32127

Upreti, B.N., Dhital, M.R., 1996. Landslide studies and management in Nepal. International Centre for Integrated Mountain Development (ICIMOD), Kathmandu, Nepal.

van Genuchten, M.T., 1980. A Closed-form equation for predicting the hydraulic conductivity of unsaturated Soils. Soil Sci. Soc. Am. J. 44, 892–898. https://doi.org/10.2136/sssaj1980.03615995004400050002x

Varnes, D.J., 1958. Landslide types and processes, in: Eckel, E.B. (Ed.), Landslides and Engineering Practice. National Academy of Sciences, Washington, D.C., pp. 20–47.

Vuillez, C., Tonini, M., Sudmeier-Rieux, K., Devkota, S., Derron, M.H., Jaboyedoff, M., 2018. Land use changes, landslides and roads in the Phewa Watershed, Western Nepal from 1979 to 2016. Appl. Geogr. 94, 30–40. https://doi.org/10.1016/j.apgeog.2018.03.003

World Bank, 2012. Nepal road sector assessment study: Annexes.

Yang, K.-H., Uzuoka, R., Thuo, J.N., Lin, G.-L., Nakai, Y., 2017. Coupled hydro-mechanical analysis of two unstable unsaturated slopes subject to rainfall infiltration. Eng. Geol. 216, 13–30. https://doi.org/10.1016/j.enggeo.2016.11.006

Yang, K.H., Nguyen, T.S., Rahardjo, H., Lin, D.G., 2020. Deformation characteristics of unstable shallow slopes triggered by rainfall infiltration. Bull. Eng. Geol. Environ. https://doi.org/10.1007/s10064-020-01942-4

Yang, K.H., Thuo, J.N., Chen, J.W., Liu, C.N., 2019. Failure investigation of a geosynthetic-reinforced soil slope subjected to rainfall. Geosynth. Int. 26, 42–65. https://doi.org/10.1680/jgein.18.00035

Yubonchit, S., Chinkulkijniwat, A., Horpibulsuk, S., Jothityangkoon, C., Arulrajah, A., Suddeepong, A., 2017. Influence factors involving rainfall-induced shallow slope failure: Numerical study. Int. J. Geomech. 17, 04016158. https://doi.org/10.1061/(ASCE)GM.1943-5622.0000865

Zhang, L., Li, J., Li, X., Zhang, J., Zhu, H., 2018. Rainfall-induced soil slope failure, Rainfall-Induced Soil Slope Failure. CRC Press Taylor & Francis Group. https://doi.org/10.1201/b20116

HIGHLIGHTS

- Poorly constructed roads cause landslides but why and how?
- Steep road cut can promote landslides during rainfall, in otherwise stable slopes
- Presence of steep roadcut lowers minimum rainfall level needed to initiate landslide
- Coupled hydro-mechanical analysis can predict timing and mechanism of landslides
- Numerical model predictions compared against field measurement improves reliability